(2)

# Optical and Physical Characteristics of the Western Alboran Sea: April 1991



**R. Hollman**
Oceanography Division
Ocean Science Directorate





## Abstract

The objective of this cruise was to characterize the bio-optical properties of the western Alboran Sea. This experiment involved the USNS BARTLETT, the R/V SEWARD JOHNSON and the JOHNSON SEA-LINK submersible (the latter two of the Harbor Research Oceanographic Institution). This technical note provides a first look report of the optical data acquired from 16 stations occupied by the USNS BARTLETT between April 2 and April 21, 1991. Results of the biological and bioluminescence experiments are covered in other reports.

Optical and physical variables of the water column were measured in three periods during the day, an a.m. period, a local noon period, and a p.m. period and included vertical profiles and time series at selected depths. Three properties are reported: the diffuse attenuation coefficient, K, derived from downwelling irradiance measurements of the natural light field, the beam attenuation coefficient, c, derived from percent transmission measurements, and fluorescence measured directly using a fluorometer. Other variables included particle sizes and concentrations, temperature and salinity, and currents.

Three composite provinces were defined based on similarities in optical properties, a southern province (Province I), an eastern province (Province II), and a northern province (Province III) with average attenuation lengths (reciprocal of attenuation coefficient, 1/K with dimensions of meters) of 13.17 m, 16.28 m, and 14.58 m, respectively. Differences between these values are statistically significant. Similar results were obtained for the distribution of particle concentrations. Clearest waters were encountered at the eastern stations, the most turbid were the southern stations, and the next in order, the northern stations. Similarly, highest concentrations of particulates were found at the southern stations, the least at the eastern stations, and next in order, the northern stations.

Temperature and salinity values were also different for each province; however, differences between the means were not consistently different. Currents observed with the Acoustic Doppler System were generally weak and in general agreement with published circulation patterns associated with an anticyclonic gyre in the western Alboran Basin.

**Acknowledgments**

The work reported herein was sponsored by CNO (OP-096) Tactical Oceanographic Warfare Support Program Office, Program Element 0603704N, Mr. Kenneth M. Ferer, NRL Detachment Code 311, Program Manager.

The diligence of Ms. P. Wagner in running the particle analysis and in the processing and analysis of those data, the support provided by Mr. M. Wilcox in programming, data acquisition and processing, and the rigging, deployment, retrieval, and maintenance of our equipment by Mr. S. Sova are all greatly appreciated. The editorial and processing help provided by Ms. L. Jugan has been of much help and is very much appreciated.

The efforts of Mr. G. Madden, Mr. J. Hedges, Mr. J. Kirby (in providing the CTD data) of the Naval Oceanographic Office, and the crew of the USNS BARTLETT are appreciated in making the cruise a successful one.

The mention of commercial products or the use of company names does not in any way imply endorsement by the U.S. Navy or NOARL.

## Contents

## Listing of Tables

## Listing of Figures

# OPTICAL AND PHYSICAL CHARACTERISTICS OF THE WESTERN ALBORAN SEA: APRIL 1991

## 1.0 INTRODUCTION

The general purpose of this cruise was to characterize the bio-optical properties of the upper waters of the Alboran Sea through measurements of the naturally occurring bioluminescence and light transmission characteristics of the surface waters. This program is in response to an insufficient data base to adequately address the requirement for a Bioluminescence Graphic for the Mediterranean Sea, and includes in its purpose, the recommendation for acquiring an adequate data set based on lessons learned.

**Table 1. Participants aboard the USNS BARTLETT during this cruise.**

| | |
|---|---|
| NOARL | |
| Dr. David K.Young | Co-Senior NOARL Representative |
| Dr. Rudolph Hollman | Co-Senior NOARL Representative |
| Mr. Dennis Lavoie | NOARL Code 333 |
| Ms. Patricia Wagner | NOARL Code 333 |
| Ms. Irene DePalma | NOARL Code 333 |
| Mr. Richard Ray | NOARL Code 333 |
| Mr. Steven Sova | NOARL Code 331 |
| OTHER AGENCIES | |
| Mr. Michael Wilcox | Planning Systems, Inc. |
| Mr. Douglas Nielson | Univ. of California (Santa Barbara) |

Station locations were chosen to cover as much of the Alboran Sea as possible within the constraints imposed by the operating depths of the JOHNSON SEA-LINK submersible and Navy operations in the area. It was intended that the USNS BARTLETT and the R/V SEAWARD JOHNSON sample the same stations with a lag of 2 days except for the central station, (Station 12, Figure 1), that was to be sampled concurrently for a period of 4 days. This station was approximately 15 nmi southwest of Isla de Alboran, and approximately 5 nmi south of the extended shallow bank that surrounds the island and extends some 30 nmi in a northeast-southwest direction. Station 11, to the north of Station 12, was just off the island and bank. The bioluminescence measurement program is addressed in a technical note by Lavoie et al. (1992); the work on the R/V SEAWARD JOHNSON is detailed in a report by Widder (1991).

The sampling program for the USNS BARTLETT had the vessel arrive on station by sunrise and remain on station for approximately 20 hr for optics and bioluminescence measurements, then proceeding to the next station. The distance between stations was generally only a few hours of steaming time.

During daylight hours, optical and environmental measurements were made in three periods, an a.m. period starting at 0800 hr, a noon period that straddled local noon (1200 hr), and a p.m. period starting at 1600 hr. Conductivity-Temperature-Depth (CTD) profiles were made between these sampling periods. Nighttime hours were devoted to bioluminescence and other biological measurements. The vessel departed station by 0600 hr or earlier, arriving on the next station before 0800 hr. Statistics for the optical measurements are tabulated in Table 2.

**Table 2. Statistics for the Optical Measurements on USNS BARTLETT Cruise 1306-91 in the Alboran Sea.**

| | |
|---|---|
| PLANNED: 17 (ONE DAY LOST TO WEATHER) | ACCOMPLISHED: 16 |
| SAMPLING PERIODS: PLANNED 51 | ACCOMPLISHED: 43 |
| CASTS: 180 (127 DOWN/53 UP) | INDIVIDUAL TIME SERIES: 525 |

A total of six sampling periods were lost due to weather, a p.m. period at Station 3, all three periods on Station 4, and the noon and p.m. periods on Station 17. One a.m. sampling period at the first Station 12 was given over to drogue tracking and retrieval. Another a.m. period was lost to transit between Stations 12 and 13 as a result of extended nighttime observations. Table 3 lists the station locations and dates. Station positions are plotted in Figure 1.

**Table 3. Station Locations for USNS BARTLETT Cruise 1306-91.**

| Station | North Latitude | West Longitude | Date |
|---|---|---|---|
| 1 | 35° 49.5' | 5° 03.8' | 2 April |
| 2 | 35° 33.5' | 4° 48.7' | 3 April |
| 3 | 35° 28.0' | 4° 27.5' | 4 April |
| 4 | 35° 27.0' | 4° 12.0' | 5 April |
| 5 | 35° 28.0' | 4° 00.0' | 6 April |
| 6 | 35° 34.0' | 3° 39.0' | 7 April |
| 7 | 35° 54.0' | 3° 21.0' | 8 April |
| 8 | 35° 35.0' | 3° 16.0' | 9 April |
| 9 | 35° 44.0' | 2° 48.0' | 10 April |
| 10 | 36° 03.0' | 2° 48.0' | 11 April |
| 11 | 35° 53.0' | 3° 01.0' | 12 April |
| 12 | 35° 45.0' | 3° 14.0' | 13-16 April |
| 13 | 36° 27.0' | 2° 57.0' | 17 April |
| 14 | 36° 29.0' | 3° 22.0' | 18 April |
| 15 | 36° 21.0' | 3° 55.0' | 19 April |
| 16 | 36° 17.0' | 4° 27.0' | 20 April |
| 17 | 36° 13.0' | 4° 59.0' | 21 April |

The general sky conditions for the western Alboran Sea for the period of the cruise, April 2 through April 21, are tabulated in Table 4.

**Table 4. General Sky Conditions During Cruise 1306-91.**

| Apr | Cloud Cover/ Description | Apr | Cloud Cover/ Description |
|---|---|---|---|
| 1 | Clear | 12 | Clear in morning increasing to 25% in evening |
| 2 | Clear | 13 | 25% in morning increasing to 100% in evening |
| 3 | Clear in morning increasing to 50% in evening | 14 | 75 - 100% cloud cover |
| 4 | 25% cloud cover | 15 | 100% in morning decreasing to 75% in evening |
| 5 | 100% cloud cover | 16 | 75% in morning decreasing to 25% in evening |
| 6 | 100% cloud cover | 17 | 25% cloud cover |
| 7 | Clear | 18 | 50% cloud cover |
| 8 | Mostly clear, some scattered clouds | 19 | 50% cloud cover |
| 9 | 25% cloud cover | 20 | 75% cloud cover |
| 10 | Mostly clear, some scattered clouds in morning | 21 | 75% cloud cover |
| 11 | Clear in morning increasing to 25% cloud cover in evening | | |

The Alboran Sea is known to contain a large clockwise gyre of surface water that enters through the Strait of Gibraltar at its western boundary and made up of North Atlantic Surface Water (Arnone et al., 1990). This gyre occupies the western portion of

the Alboran Sea. The eastern portion also contains a clockwise gyre made up of Mediterranean Water mixed with North Atlantic Water. Isla de Alboran appears to be on the dividing line between the two gyres, so that Stations 8, 11, and 12 are probably influenced by any interaction between them.

Measurements of the optical properties of the water column were made using two MER 2040 systems manufactured by Biospherical Instruments Inc., mounted to a modified rosette frame. One MER unit has 19 sensors and a timer; 16 of the sensors are spectral vector irradiance sensors, 8 for the downwelling irradiances and 8 for the upwelling irradiances. In addition, this unit also contains the pressure, tilt, and roll sensors. The second unit contains 12 sensors and a timer. Six of these sensors are for the spectral scalar downwelling irradiances, and six for the spectral scalar upwelling irradiances. Four external sensors are connected to the first MER 2040 unit and are for the SEA BIRD temperature, conductivity, and pressure sensors and a SEA TECH fluorometer. The second unit at present has only one external sensor, a SEA TECH 25 cm path length transmissometer operating at 660 nm. Analog signals both from external and internal sensors are sequentially sampled and converted to digital form and stored along with time in the MER 2040 internal memory until requested by an on deck computer. Both MER's share the serial data link to the deck unit. The SEA BIRD sensors are frequency devices and are measured by the MER's period averaging circuitry and added to the data stream. The sampling rate is 13 Hz with the exception of the surface light sensors that are sampled at 1 Hz and converted to digital signal in the deck unit and then added to the data stream to the data acquisition computer. These sensors are tabulated in Table 5.

**Table 5. Tabulation of the Optical Sensors on the MER 2040 System.**

| Spectral Vector Irradiance ($\mu w/cm^2$ - nm) | Sensors |
|---|---|
| $E_d$ 410/441/465/488/520/560/589/656 - downwelling | (16) |
| $E_u$ 410/441/465/488/520/560/589/656 - upwelling | |
| Spectral Scalar Irradiance ($\mu w/cm^2$ - nm) | |
| $Eo_d$ 441/488/520/560/589/656 - downwelling | (12) |
| $Eo_u$ 441/488/520/560/589/656 - upwelling | |
| Transmissometer - (% Transmission) | |
| Fluorometer - (volts) | |
| Tilt (degrees) | (5) |
| Roll (degrees) | |
| Pressure (decibars) | |
| Deck Cell - Irradiance (Vector) ($\mu w/cm^2$ - nm) | |
| SL 410/488/550/683 - Solar plus Sky Radiation | (4) |
| Total | (37) |

## 2.0 RESULTS

### 2.1 Optics Measurements

One-hundred-eighty optics casts were made during this cruise not including the time series measurements. Thirty-seven variables are measured at approximately 13 Hz including pressure, so that there are 36 pressure dependent variables; therefore, for 180 casts, there are 6480 individual profiles to be displayed. To reduce this number, only representative profiles from each sampling period for the 17 stations were selected for discussion in this technical note.

The first column of vertical plots in these figures is for the beam attenuation coefficient, c, with units of $m^{-1}$, and is calculated from the percent transmission as measured with the SEA TECH transmissometer operating at 660 nm. The second column is for the fluorescence as measured by the SEA TECH fluorometer in volts and represents a relative measure of the pigment concentration in the water column. The last column of plots is for the diffuse attenuation coefficient, K, with units of $m^{-1}$, and is calculated from the downwelling vector irradiance. In the examples shown, the values for K are at 488 nm, the wavelength of maximum penetration in the Alboran Sea. The definition for K is given by:

$$K(488;z) = -(1/(z_2 - z_1) * \ln(Ez_1 - E(z_2)) \quad (1)$$

where E is the downwelling vector irradiance at 488 nm for depths $z_1$ and $z_2$. The units for E are microwatts/cm$^2$/nm, the units for K are m$^{-1}$.

Figure 2 shows the three variables, c, fluorescence, and K, for Station 1. The missing plot for the a.m. c was caused by a data logging error that was corrected when discovered. In general, the profiles for c and fluorescence are noisy and not strongly correlated, implying that not all of the particles were pigment bearing. Since the variability in the irradiance field is partly related to the particle composition and concentration, the attenuation coefficient, K, calculated from the gradient of the downwelling irradiance, is going to reflect this variability even more strongly. This is demonstrated by the noisy K profile. The rapid falling off of K with depth at the bottom of the profile is caused by the instability in the calculations when the irradiance values approach the dark current values. Dark current values are measured daily to track sensors that may begin to malfunction and drift and in effect, is the background system noise in the sensor channel.

Figure 3 shows the variables for Station 2. In this case, the profiles are much less noisy and indicate a two layer system with a relatively turbid mixed layer with high concentrations of particles and particles with high pigment concentrations overriding a clearer layer. The upper mixed layer extends to approximately 50 m throughout the day. In the lower layer, values of c and K have been reduced by a factor of 2 from their values in the mixed layer and fluorescence decreased by an order of magnitude. There is a noticeable layering in these fluorescence profiles that is not apparent in the profile of c, indicating that the layers are composed of different types of organisms at approximately the same concentration.

At Station 3, the same general picture was obtained (Figure 4). A relatively turbid mixed layer extending down to 50 m resting on top of a much clearer layer. In the a.m. series, the layering effect in the fluorescence profile also appears in the c profile although at different depths, again indicating layering involving different particle concentrations in the case for c and in different pigment concentrations in the case of the fluorescence. These effects are seen in the attenuation coefficient profile. The p.m. series was dropped due to the onset of gale force winds that lasted throughout the next day.

The next station, Station (5), presented in Figure 5, shows the effect of the strong winds in the deepened mixed layer to approximately 85 m. The layering in the fluorescent profile is still apparent indicating that the organisms are not completely dominated by the vertical mixing induced by wave action at the surface. Corresponding particle concentrations are much more uniform, thus implying that the particle concentration is almost

constant with depth in this mixed layer as compared to the pigment concentration. Particulates at 55 m had a high concentration of pigments as can be seen in the fluorescence profile.

A shallow layer of high particle concentration (high c values) together with high pigment values (high fluorescence) extends down to 25 m at Station 6, shown in Figure 6. The fluorescence appears to increase in magnitude and thickness throughout the day, whereas the particle concentrations appear to remain constant. These effects are to be seen in the corresponding K profiles.

A much stronger fluorescence signal and increased particle concentration can be seen in Figure 7, Station 7. Here, the fluorescence peak is at 35 to 40 m while the peak of the particle concentration is at the surface with a secondary peak at 28 m. The resulting K profile however, matches the fluorescent distribution. The peak in fluorescence in the p.m. series has gone down to 50 to 55 m and is also shown in the K profile. In general, the K profiles show K to be relatively large, on the order of 0.12 to 0.15 $m^{-1}$ in the surface layer (variable extending down to 70 m in some cases) and rapidly falls off to approximately 0.03 $m^{-1}$. In comparison, these subsurface values are comparable to K values from the Sargasso Sea.

The corresponding profiles obtained from Station 8 are shown in Figure 8. The a.m. profiles show a much stronger correlation between the values for c and fluorescence, with both variables indicating a well mixed surface layer down to 35 m. This correlation weakens with the increased solar radiation in the noon series and probably represents an example of photoinhibition affecting the phytoplankton in the surface layer. The K profiles again reflect the distributions of c and fluorescence. The fall off of K at the bottom of the a.m. profile again indicates the low energy levels encountered at 100 m in the early morning hours, thus producing instability in calculating the gradients for determining K.

Values for fluorescence and c were lower by more than a factor of 2 in the observed variables at Station 9 (Figure 9). Corresponding K values are also lower by 25% in comparison to Station 8. The day was generally overcast with occasional breaks in the clouds. This condition is reflected in low values of irradiances in the water column and results in instabilities in numerical values of the vertical gradient used in calculating K. This produces the sharp variations that can be seen in the lower portion of the p.m. K profile.

Fluorescence values at Station 10 were even lower than at Station 9 at the start during the a.m. observations as shown in Figure 10. The K values were also lower(compare 0.07 at Station 10 with 0.09 at Station 9). Surface values for fluorescence remained low throughout the day and almost matched the low values generally observed beneath the mixed layer. The fluorescence maximum also remained at the same depth of 40 m during the day. A shoulder

(small secondary maximum) can be observed at approximately 70 m on the a.m. profile and became more pronounced as the day progressed. The cover used to monitor the dark current of the transmissometer was inadvertently left on during the first cast and therefore no values were reported for the c profiles in the figure.

The profiles from Station 11, just off the bank that forms the Ilsa de Alboran, are very similar to those of Stations 9 and 10, thus indicating the same water mass. The profiles for this station are shown in Figure 11 and were obtained by sampling at a drogued drifter rather than at a fixed location; however, the drogue appeared to be caught up in a small gyre of approximately 5 nmi in diameter so that the profiles obtained were not far from the starting point at anytime during the day-long sampling.

Station 12 was sampled for 4 consecutive days, April 13 through April 16 and results are shown in Figures 12 through 15. It is apparent from an examination of Figures 12 and 13, the first 2 days at Station 12, that the water mass encountered during this period is different from the one encountered at Stations 9,10, and 11. Fluorescence is again much higher and more in line with values observed at Station 7 and 8 for the a.m. series. The highest values of fluorescence for the Alboran Sea were encountered during the second day at Station 12 on April 14 when values exceeded 2V. Values for the beam transmission, c, were also high but matched maximum values with Station 7, and were slightly in excess of 0.09 $m^{-1}$. The highest values for K (at 488 nm) greater than 0.15 $m^{-1}$ were also observed during this period and again points out the strong correlation between K and the particulates and the pigments. Conditions changed for the third and fourth days (April 15 and 16), when values for these variables were observed to be lower and more in line with the values encountered at the earlier stations. The profiles also resemble those observed at Stations 9, 10, and 11; however, the depth of the maxima in c and fluorescence are shallower at this station than at Stations 10 and 11 (approximately 30 m compared to 45 m).

Profiles for Station 13 are shown in Figure 16 for April 17. The a.m. observation series was given over to transit between Station 12 and 13, and resulted from extended night observations that ran into the early morning hours of April 17. Here, the maxima in c and fluorescence are deeper, centered at 42 m as compared to approximately 20 m during the last day at Station 12 (April 16, Figure 15). The magnitude of these maxima are virtually the same as at Station 12; however, they are not only deeper but also more extensive, reaching some 40 m in thickness compared to 25 m at Station 12.

Station 14, Figure 17, is interesting in that the upper mixed layer as indicated by the c profile remains relatively constant throughout the day extending only to 30 m. The maximum in the fluorescence profile deepens from 30 m in the a.m. series to 70 m by the time of the p.m. series, and appears to be the result of growth or vertical migration of the organisms in the secondary maximum at the expense of the organisms in the shallower primary

maximum in the a.m. and noon series. This downward shift in the fluorescence maximum is borne out in the K profile that well mirrors this effect.

At Station 15 (Figure 18), however, the surface maximum in fluorescence remains at the surface (25 m) throughout the day. The secondary maximum varies in depth from 85 m in the a.m. series to 65 m during the noon series, to approximately 80 m again during the p.m. series. This migration of the secondary peak is also well marked in the c profile and follows the migration pattern established in fluorescence distribution. The resulting K profile dramatically shows the influence of these distributions. It is also noted that this secondary peak both in the c and fluorescence profiles broadens out during the day from approximately 5-m thick to about 20 m. The level of particulated concentrations in the upper layer are comparatively high (0.8 $m^{-1}$) with the secondary maximum (0.55 $m^{-1}$) at depth causing the lower level to have a relatively high concentration as well.

Figure 19 shows the profiles for Station 16 on April 20. The high concentrations of particulates and fluorescence are confined to the a very shallow and thin upper layer centered at 20 m during the a.m. series. These maxima increased, broadened, and were centered at 35 m during the noon series. During the p.m. series, they became shallower again (25 m), but increased in magnitude (over 2V for the fluorescence) and in the case for the particulates, became more concentrated (thinner). K profiles reflect these distributions with maximum value of almost 0.12 $m^{-1}$ during the p.m. series.

Station 17 has only an a.m. series, as shown in Figure 20. The remaining measurements were canceled due to the onset of gale force winds. At this station, the particulate concentration is very broad and deep with a narrow maximum centered at 50 m. The fluorescence profile shows three maxima, the first centered at 10 m, another at 50 m, with the primary maximum at 60 m. There is also a hint that another maximum is developing at 90 m and also shows up in the resulting K profile at 90 m. The main peak in the K profile also occurs at 50 m.

In summary, the stations on the southern rim of the Alboran Basin had more extensive or broader particulate and fluorescence distributions than either the stations on the northern rim of the basin or in the central region (refer to Figure 1). The central stations appeared to be different from either the southern or northern stations.

The requirements of the personnel doing the nighttime camera work from aircraft overflights were for optical characterization in terms of attenuation lengths, the reciprocal of the attenuation coefficient defined in equation (1), that is, if L is the attenuation length, then $L = 1/K$ with units of meters. From the results shown in the distributions for the 17 stations (Figures 2 through [illegible]), a hint that the stations could be divided into provinces that displayed similar characteristics in optical

properties needed a more quantitative foundation. To attain this, an index was calculated and was simply the average attenuation coefficient derived from the integrated vertical distribution then divided by the maximum depth:

$$Average\ K = 1/D\int_o^D K\ (488;z)\ dz, \qquad (2)$$

where the integration extends from the surface to 100 m so that D = 100 m. The attenuation coefficients used to calculate the vertical averages were derived from the time series profiles. The vertical averages were then simply averaged for each station and L, the attenuation length, calculated from these station averages. The average attenuation coefficients and the corresponding average attenuation lengths for each station are tabulated in Table 6 and displayed in Figure 21 by station location.

**TABLE 6. Statistics as Calculated from MER Measurements.**

$$Mean\ Attenuation\ Coefficient\ K = 1/100\int_o^{100m} K(488;z)\ dz \qquad (3)$$

| Station Number (Number of Casts) | | Mean Attenuation Coefficient ($m^{-1}$) | | Attenuation Length |
|---|---|---|---|---|
| 1 (3) | | 0.0864 | | 11.51 |
| 2 (3) | | 0.0683 | | 14.65 |
| 3 (1) | | 0.0824 | | 12.13 |
| 5 (3) | | 0.0770 | | 12.98 |
| 6 (5) | | 0.0702 | | 14.25 |
| 7 (5) | | 0.0865 | | 11.56 |
| 8 (5) | | 0.0784 | | 12.75 |
| 9 (6) | | 0.0602 | | 16.00 |
| 10 (3) | | 0.0616 | | 16.22 |
| 11 (3) | | 0.0647 | | 15.46 |
| 12 (11) | | 0.0716 | | 13.97 |
| 13 (1) | | 0.0583 | | 17.14 |
| 14 (3) | | 0.0688 | | 14.53 |
| 15 (3) | | 0.0691 | | 14.47 |
| 16 (3) | | 0.0668 | | 14.97 |
| 17 (1) | | 0.0719 | | 13.91 |
| Total: (59) | Average: | 0.0716 | Average: | 13.96 |

It can be seen in Table 6 and Figure 21 that the highest station averages occurred at the eastern stations, in particular, Stations 9, 10, 11, and 13. These stations were therefore averaged as a composite area. Similarly, the northern stations (Stations 14, 15, 16, and 17) were averaged as were the southern stations (Stations 1 through 8 and 12). The results of this compositing is shown in Figure 22 and tabulated in Table 7.

**TABLE 7: Mean Values for Physical Properties in Provinces I, II, and III**

Province I consists of Stations 1 through 8, and 12.
Province II consists of Stations 9, 10, 11, and 13.
Province III consists of Stations 14, 15, 16, and 17.

| PROPERTY | PROVINCE I | PROVINCE II | PROVINCE III |
|---|---|---|---|
| Mean Attenuation Coefficient (K) | 0.0759 $m^{-1}$ | 0.0614 $m^{-1}$ | 0.0686 $m^{-1}$ |
| Mean Attenuation Length (L) | 13.17 m | 16.28 m | 14.58 m |

These province means were tested to determine if there was a significant difference between them. For Provinces I and II, comparing the southern province with the eastern province, the means are significantly different to the 0.2% level; for Provinces I and III, here comparing the southern province with the northern province, the means were also found to be different to the 0.2% level; and, for Provinces II and III, comparing the eastern province with the northern province, the means were significantly different to the 1% level. In other words, the chance of making an error is 1 in 500 and 1 in 100, respectively.

## 2.2 Temperature and Salinity Measurements

Two CTD casts were made each day, the first between the a.m. and the noon series of optics measurements and the second between the noon and the p.m. optics series. The profiles are shown in Figures 23 through 31. There are no profiles for Stations 3 and 4 as a result of weather conditions. Temperature inversions are notable in Stations 1 (near surface), 9, 11, 12, 13, and 17. The most striking inversion occurred at Station 9 during both casts, had a temperature increase of 0.25°C approximately 10-m thick, and centered around 75-m depth (Figure 26). Some small steppiness can also be seen in these profiles particularly for Stations 2 and 17 (Figures 23 and 31, respectively).

In general, there were two water masses present in the western Alboran Basin, an upper water mass with an average temperature of 15.512°C and an average salinity of 36.485 psu. The second water mass occupied the bottom portion of the Alboran Basin and had an average temperature of 13.248°C and an average salinity of 38.267 psu obtained at the thermocline and halocline depths, respectively.

Average temperatures and salinities for the surface and at the thermocline and halocline along with their respective depths are tabulated in Table 8 for the three provinces defined by the attenuation lengths (Table 7). As can be noted in Table 8, the coolest surface water was in Province II, the warmest was in Province III with a difference of 0.228°C. Higher average saline water was also found in Province II with the lower salinity in Province I for a difference of 0.331 psu. The only significant difference in the average temperatures is between Province II and III; the differences between the average temperatures between Provinces I and II and between Provinces I and III are not significant. The differences between the average surface salinities for the three provinces are significantly different. Average thermocline temperatures show a smaller range of 0.124°C with Province I being the coolest and the deepest (215.6 m) with Province III the warmest and shallowest thermocline depth (160.2 m). Significant differences between the average temperatures were found for Provinces I and III, and Provinces II and III. In the case of salinity, the only significant difference between average salinities is between Provinces II and III. However, the depths at which the thermocline and halocline occur are significantly different between provinces with the exception of the average halocline depths between Provinces II and III.

Temperature differences between the surface and the thermocline were approximately 2.5°C and approximately 2 psu between the surface and halocline.

**Table 8. Average Temperatures and Salinities for the Surface of Thermocline and Halocline, with their average depths, for the three provinces.**

Province I consists of Stations 1 through 8, and 12.
Province II consists of Stations 9, 10, 11, and 13.
Province III consists of Stations 14, 15, 16 and 17.

| | Average Surface | | Average Thermocline | | Average Halocline | |
|---|---|---|---|---|---|---|
| Province | Temp(°C) | Sal(psu) | Temp(°C) | Depth(m) | Temp(°C) | Depth(m) |
| I | 15.513 | 36.402 | 13.192 | 215.6 | 38.263 | 192.7 |
| II | 15.393 | 36.733 | 13.234 | 190.3 | 38.287 | 171.6 |
| III | 15.621 | 36.503 | 13.316 | 160.2 | 38.252 | 150.6 |

## 2.3 The Distribution of Particulates

A Particle Data Inc., EL-ZONE Model 80-XY particle counter, was used to determine particle counts and equivalent volume from water samples drawn from selected depths during each sampling session. The EL-ZONE particle counter operates on the Coulter

principle. Three different orifices were used to process the samples and the results blended to produce particle size distributions between 1 and 100 μm. A total of 101 water samples were processed for the western Alboran Sea. The purpose of these measurements was to identify a baseline for defining the interaction between particles and the natural light field in water column.

A Junge type distribution (also called hyperbolic) was calculated from the particle size distribution for each sample (for example see Bader, 1970). An example is shown in Figure 32 where the logarithm to base 10 of the cumulative particle size is plotted against the logarithm to base 10 of the particle diameter. Here, the ordinate represents the log of the number of particles greater than the corresponding particle diameter shown on the abscissa. The number of small particles is in general greater than the number of larger particles in any given sample, therefore the slope is always negative with the highest concentrations appearing at the lowest end of the abscissa (zero representing the log of 1 μm).

A regression analysis was performed on each distribution and is shown on the example in Figure 32. The intercept, or offset, represents the total particulate concentration for that sample. These results were also grouped as to stations as was done previously. Results of this grouping are tabulated in Table 9.

**Table 9. Average slopes and offsets derived from regression analysis of the particle distributions for each of the provinces.**

Province I consists of Stations 1 through 8, and 12.
Province II consists of Stations 9, 10, 11, and 13.
Province III consists of Stations 14 through 17.

| Parameter | Province I | Province II | Province III |
|---|---|---|---|
| Slope | -2.948 | -3.004 | -3.015 |
| Offset(*) | 10.893 | 10.755 | 10.882 |
| | ($7.8163 \times 10^{10} l^{-1}$) | ($5.6885 \times 10^{10} l^{-1}$) | ($7.6208 \times 10^{10} l^{-1}$) |

(*) The offset represents the total particle concentration. Figures in parentheses are the antilog of the offsets, and have units of particles per liter.

The differences between the slopes for each province are not significant; however, the average offsets or total particle concentrations, are significantly different at better than the 5% level, and in good agreement with the results for the attenuation lengths in these provinces, as would be expected since particulates are the dominant factor in the attenuation of the natural light field.

## 2.4 Currents

A RD Instruments Vessel Mount (RD-VM) Acoustic Doppler Current Profiler (ADCP) was installed in the through hull well of the USNS BARTLETT. It consists of a transducer unit in the hull that is connected via cable to an electronics unit coupled to a data acquisition system including input from the ship's gyro compass and satellite navigation system. Problems with adjusting the results for ship's speed have not been resolved at this writing, therefore results are only presented for the times when the vessel was hove-to with speeds of 0.5 kt or less as was the case when measurements were being made.

Examples of the profiles for 1-hr averages during the period of 0800 and 1800 hr and when the vessel's speed was less than or equal to 0.5 kt are shown in Figure 33. Figure 33 (a) shows the results for Station 17 near the Strait of Gibraltar and what should be the beginning of the clockwise gyre. The flow, however, is fairly strong (0.85 kt) to the south with a westerly component opposite to the expectation of a flow to the northeast or east if the gyre were established. Winds during this day became gale force from the west-northwest and could possibly have masked or altered the flow associated with the gyre. Figure 33 (b) shows the results for Station 11 in the middle of the Alboran Basin. The gyre should be absent in this area having already swung to the south; therefore, a very weak and variable flow is expected and was so observed with both profiles (north/south and east/west) hovering about zero. Figure 33 (c) shows the two profiles for Station 1 near the southern side of the Strait of Gibraltar (Figure 1). Here the flow is mostly to the west with a weak northerly component, in the direction of the Strait, indicating a portion of the gyre is breaking off to eventually bebouch into the Atlantic.

## 3.0 CONCLUSIONS

The average attenuation coefficient, K, for the western Alboran Sea is 0.0716 $m^{-1}$ with a corresponding attenuation length of 13.96 m, based on data from all stations. This indicates a Jerlov Case II classification for the Alboran Sea.

This average K value is in general, more than a factor of 2 greater than values representing the Sargasso Sea for example (K near 0.030 $m^{-1}$ and attenuation length near 33.3 m), yet not as high as might be encountered in near-shore or estuarine conditions (K near 0.200 $m^{-1}$ and attenuation length near 5 m).

Stations in the Alboran Sea could be grouped according to their average attenuation lengths, or their average attenuation coefficients (refer to Table 6) into three provinces: a southern province (Province I), an eastern province (Province II), and a northern province (Province III) with average attenuation lengths of 13.17 m, 16.28 m, and 14.58 m, respectively. These mean values are significantly different to better than the 1% confidence level. Similar results for bioluminescence were reported by Lavoie et al. (1992).

Optical characteristics of the water column depend in large measure upon the nature and concentration of particulates. It would follow, then, that the particle concentrations would also fall into the same three provinces, and so they did. Province II had the highest attenuation lengths, therefore the clearest waters and also the lowest concentration of particles (Table 9). Province III was next in attenuation length, hence water clarity, and also had the next higher concentration of particles per liter of water. Province I was the most turbid (attenuation length of 13.17 m) and also had the highest number of particles. The fact that the slopes of the cumulative frequency distributions (Figure 32 and Table 9) were not significantly different for the three provinces indicates that the distribution of particle diameters is uniform in the western Alboran Sea. In other words, the ratio of small to large particles remains constant from one province to the other.

The Alboran Basin can be characterized as a two-layered system with a warmer and less saline water mass of average temperature 15.51°C and a temperature 13.25°C and salinity 38.27 psu, the later determined at the thermocline and halocline depths, respectively. Provincing of the thermocline and halocline depths did agree with the results indicated by the optical and particle distributions in that the difference between the average depths in all three provinces were found significantly different except for the differences between the halocline depths in Provinces II and III, the central and northern provinces, respectively.

Currents measured with the ADCP while the ship was hove-to on station revealed generally low velocities especially in the central stations of Province II. The largest velocities were recorded at Station 17; however, these can be attributed to the gale force winds that prevailed on that day (April 21, 1991).

## STATION STATISTICS

**Planned: 17**
**Accomplished: 16**

**Sampling Periods: 51**
**Accomplished: 43**

**Casts: 180**

**Individual Time Series: 525**



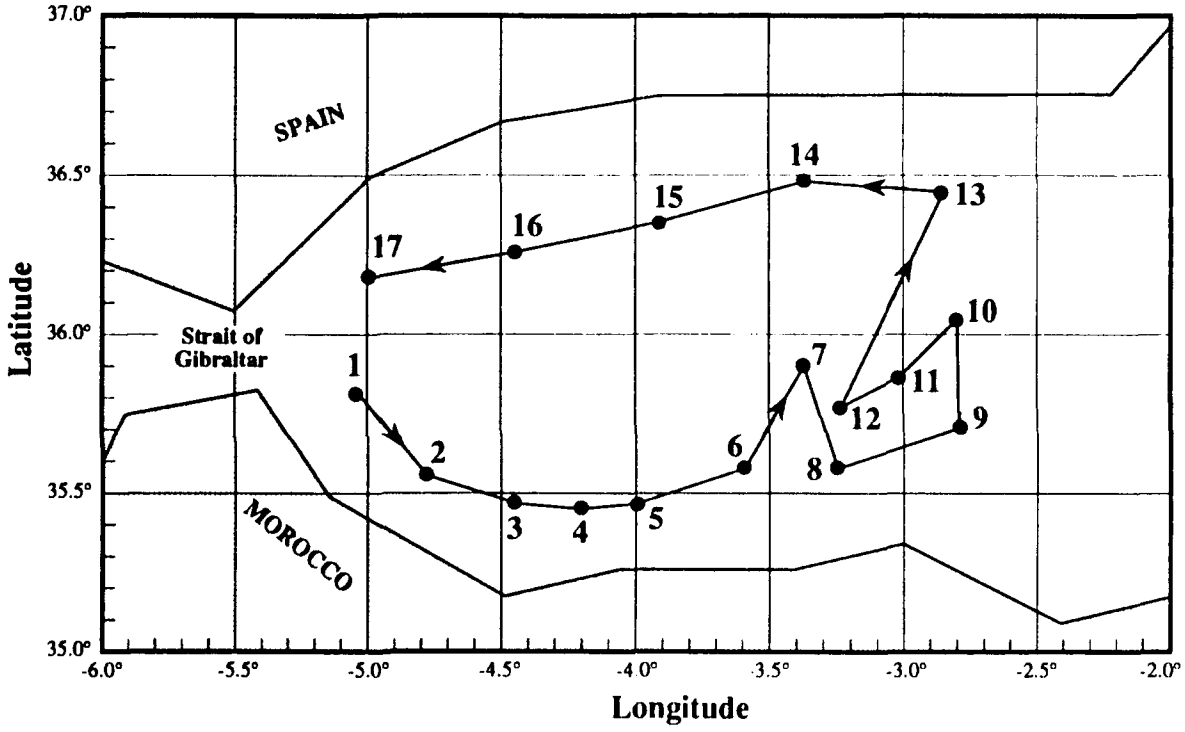


**Figure 1. Station Locations and Track of USNS BARTLETT Cruise 1306-91.**

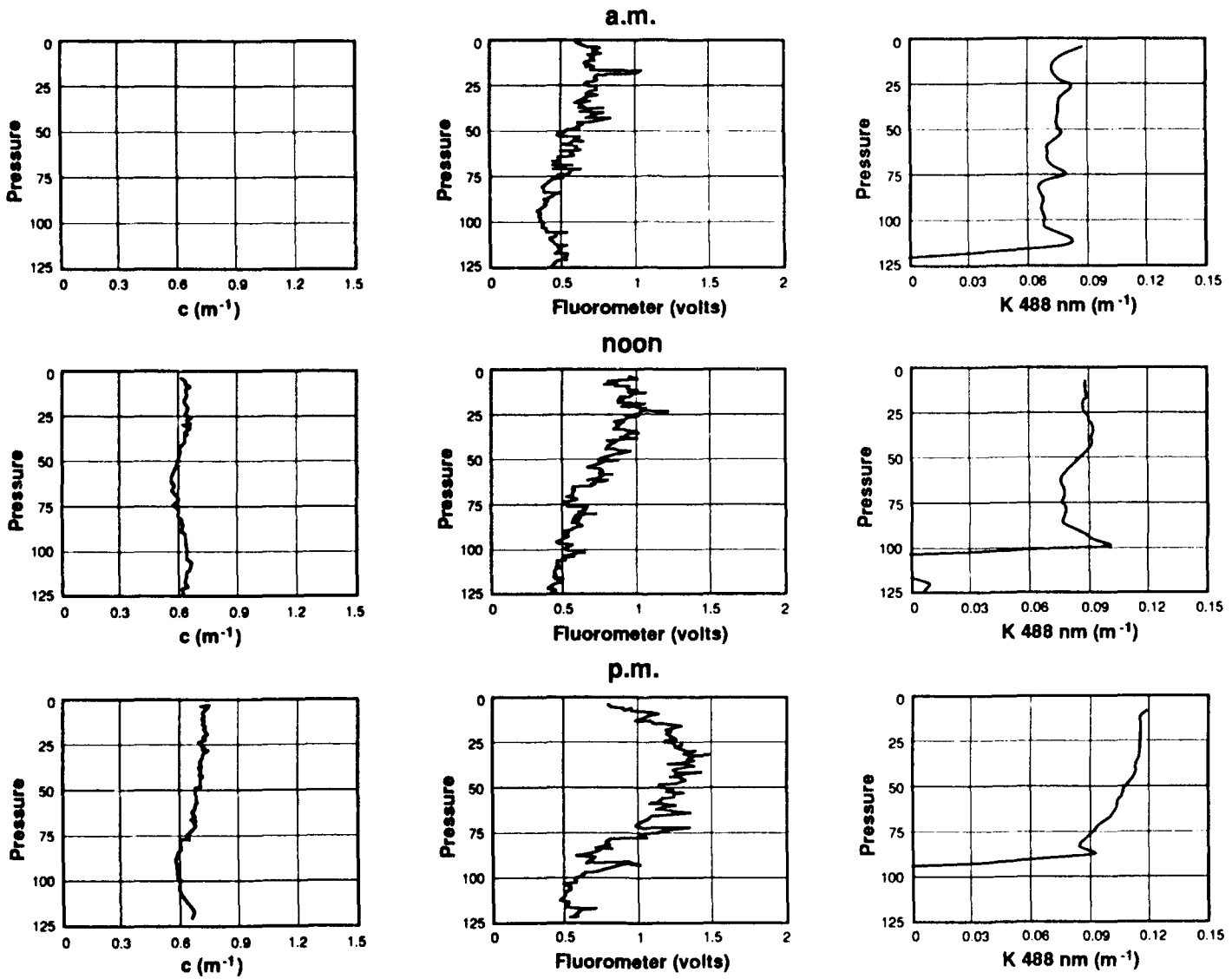


**Figure 2. Representative profiles taken from the a.m., noon, and p.m. sampling periods for Station 1. C is the beam attenuation coefficient with units of $m^{-1}$, the fluorometer measurement is relative and is in volts, and K 488 is the attenuation coefficient calculated from irradiance profiles and also has units of $m^{-1}$.**

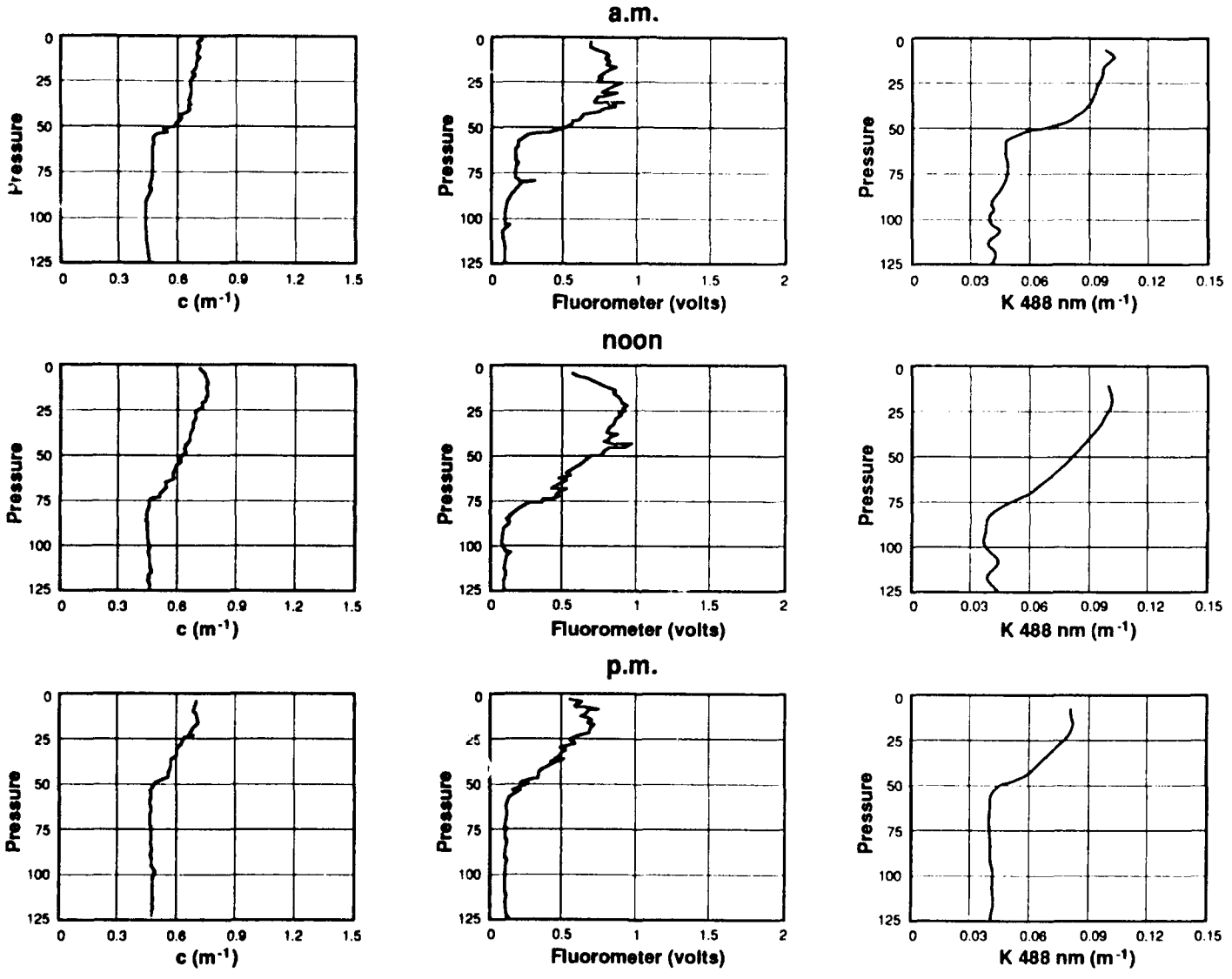


**Figure 3. Representative profiles taken from the a.m., noon, and p.m. sampling periods for Station 2. C is the beam attenuation coefficient with units of $m^{-1}$, the fluorometer measurement is relative and is in volts, and K 488 is the attenuation coefficient calculated from irradiance profiles and also has units of $m^{-1}$.**

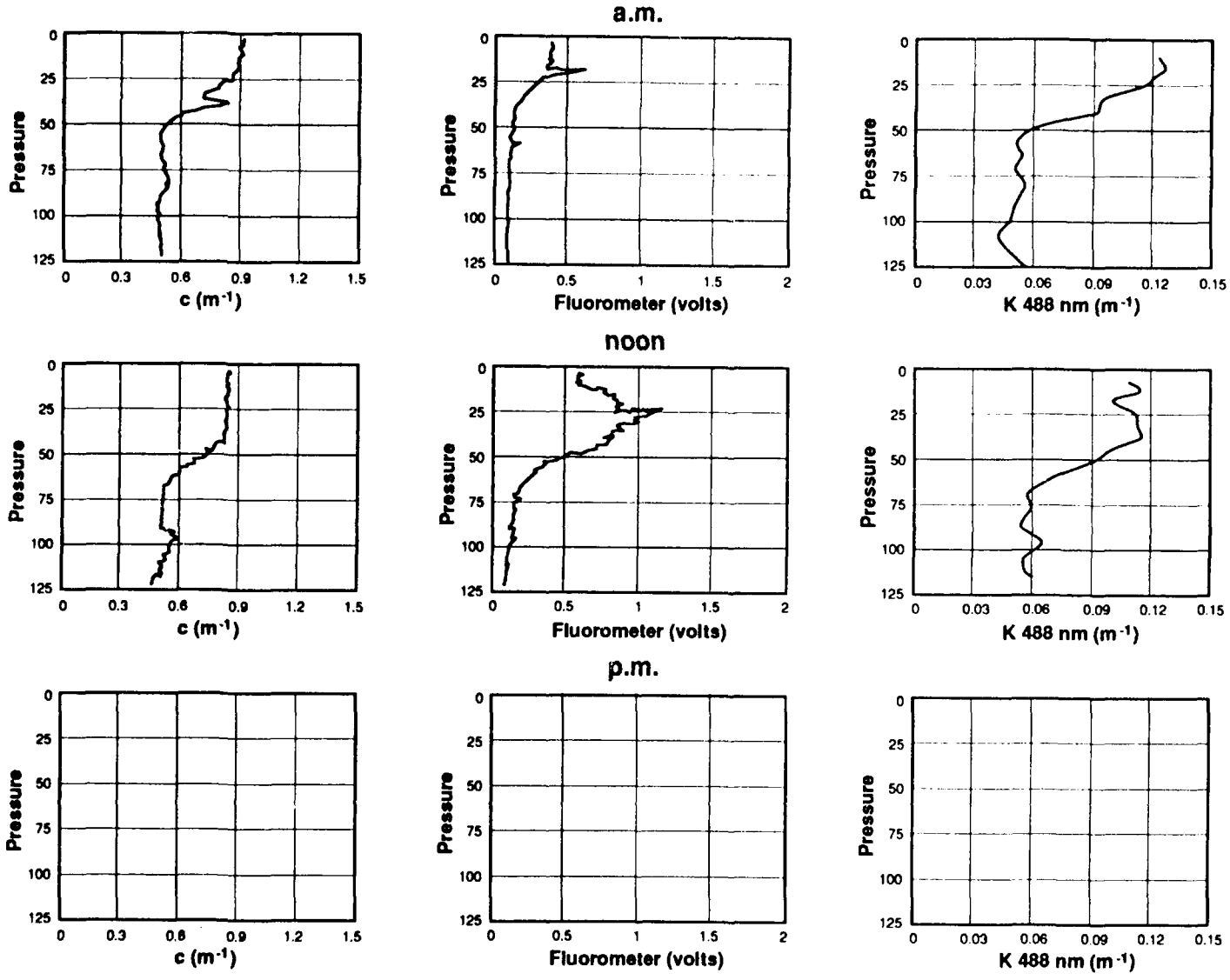


**Figure 4. Representative profiles taken from the a.m., noon, and p.m. sampling periods for Station 3. C is the beam attenuation coefficient with units of $m^{-1}$, the fluorometer measurement is relative and is in volts, and K 488 is the attenuation coefficient calculated from irradiance profiles and also has units of $m^{-1}$.**

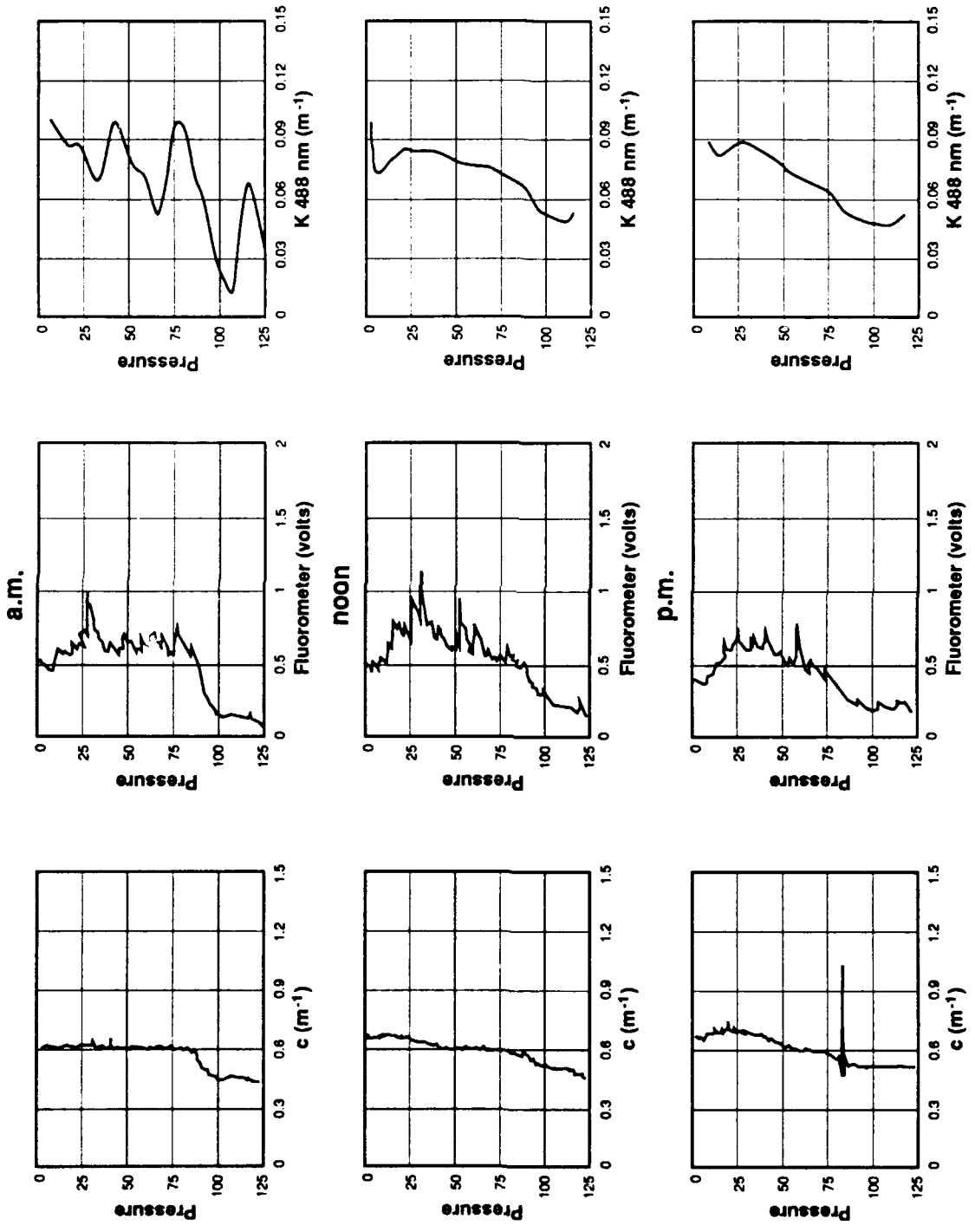


**Figure 5. Representative profiles taken from the a.m., noon, and p.m. sampling periods for Station 5. C is the beam attenuation coefficient with units of $m^{-1}$, the fluorometer measurement is relative and is in volts, and K 488 is the attenuation coefficient calculated from irradiance profiles and also has units of $m^{-1}$.**

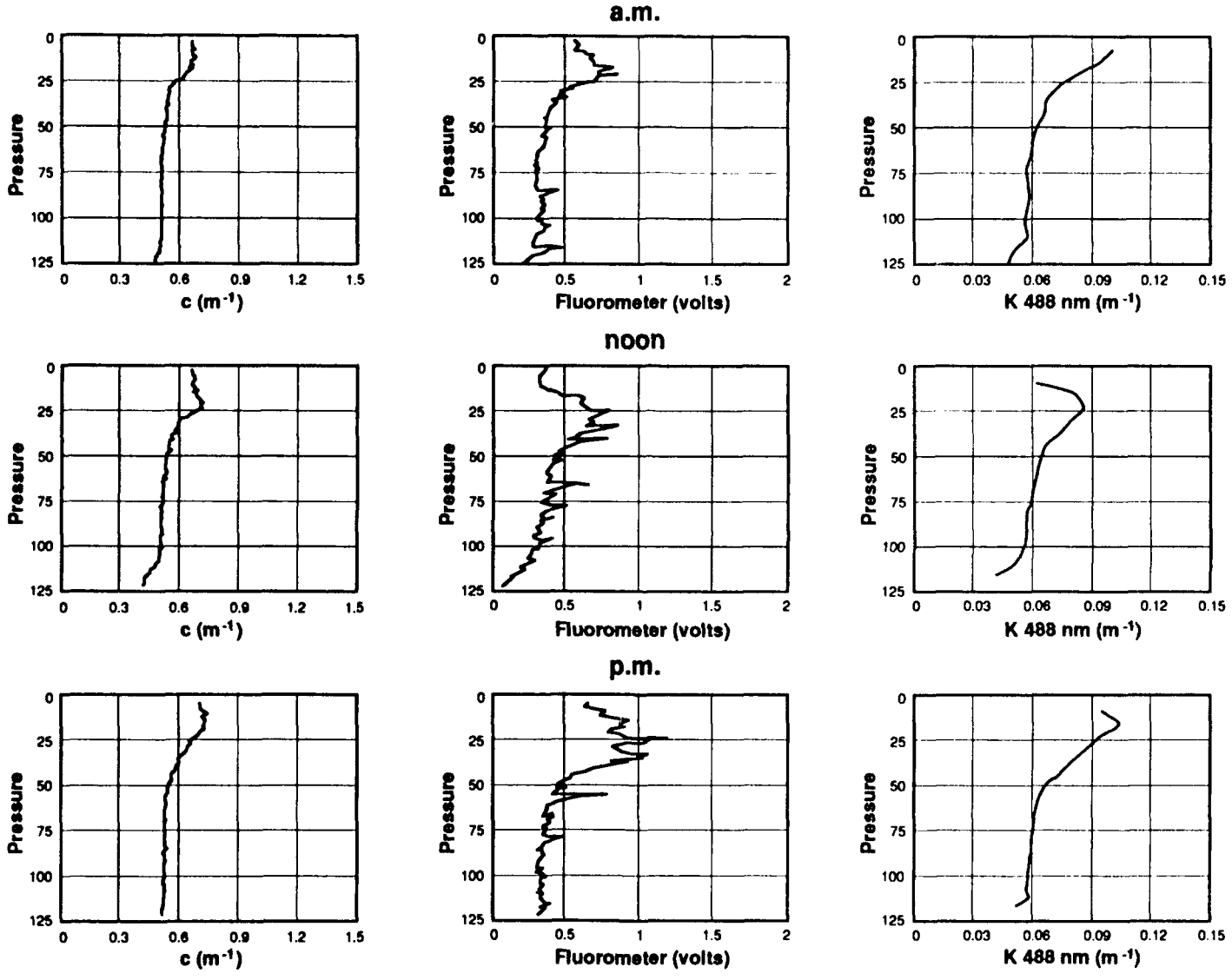


**Figure 6. Representative profiles taken from the a.m., noon, and p.m. sampling periods for Station 6. C is the beam attenuation coefficient with units of $m^{-1}$, the fluorometer measurement is relative and is in volts, and K 488 is the attenuation coefficient calculated from irradiance profiles and also has units of $m^{-1}$.**

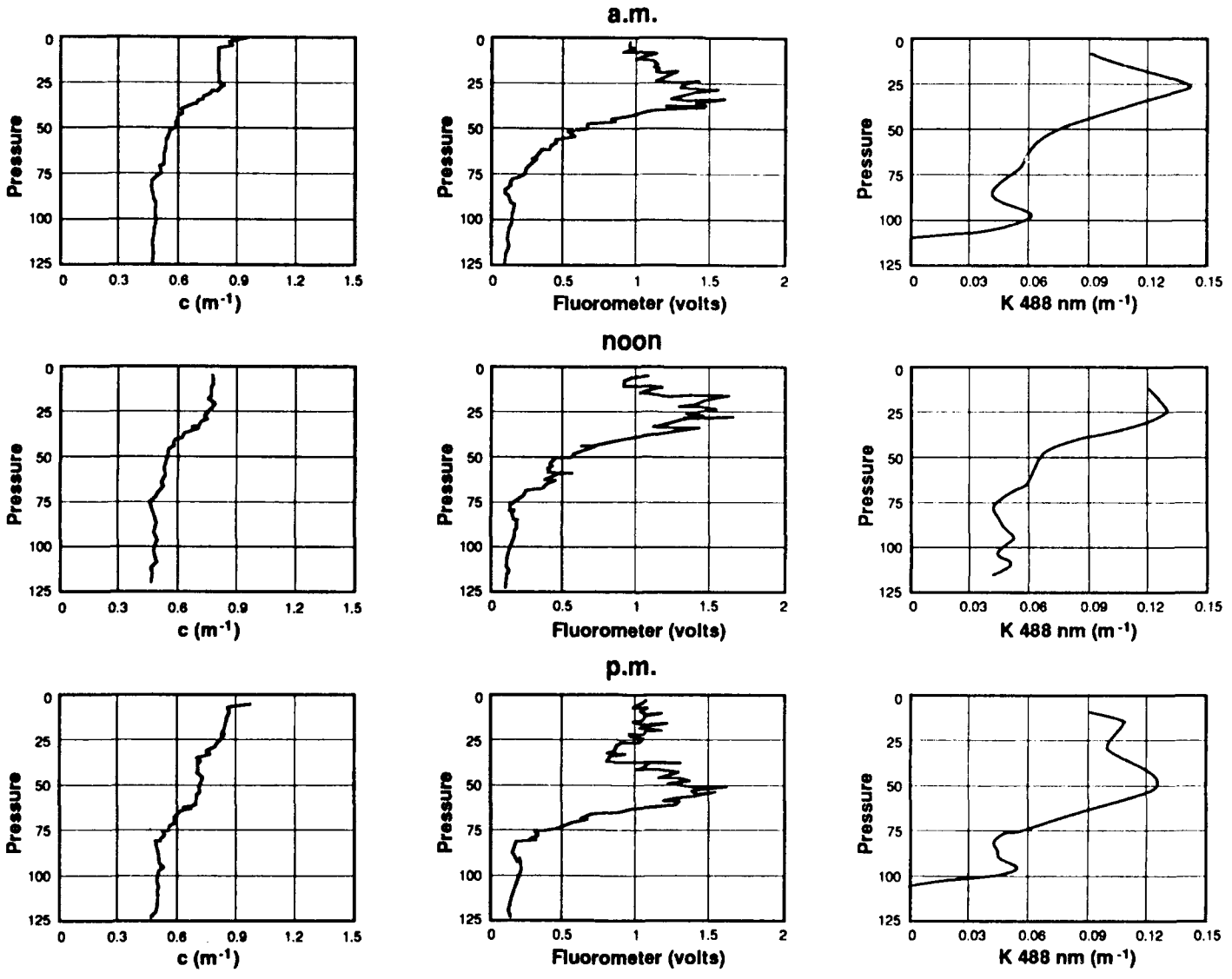


**Figure 7. Representative profiles taken from the a.m., noon, and p.m. sampling periods for Station 7. C is the beam attenuation coefficient with units of $m^{-1}$, the fluorometer measurement is relative and is in volts, and K 488 is the attenuation coefficient calculated from irradiance profiles and also has units of $m^{-1}$.**

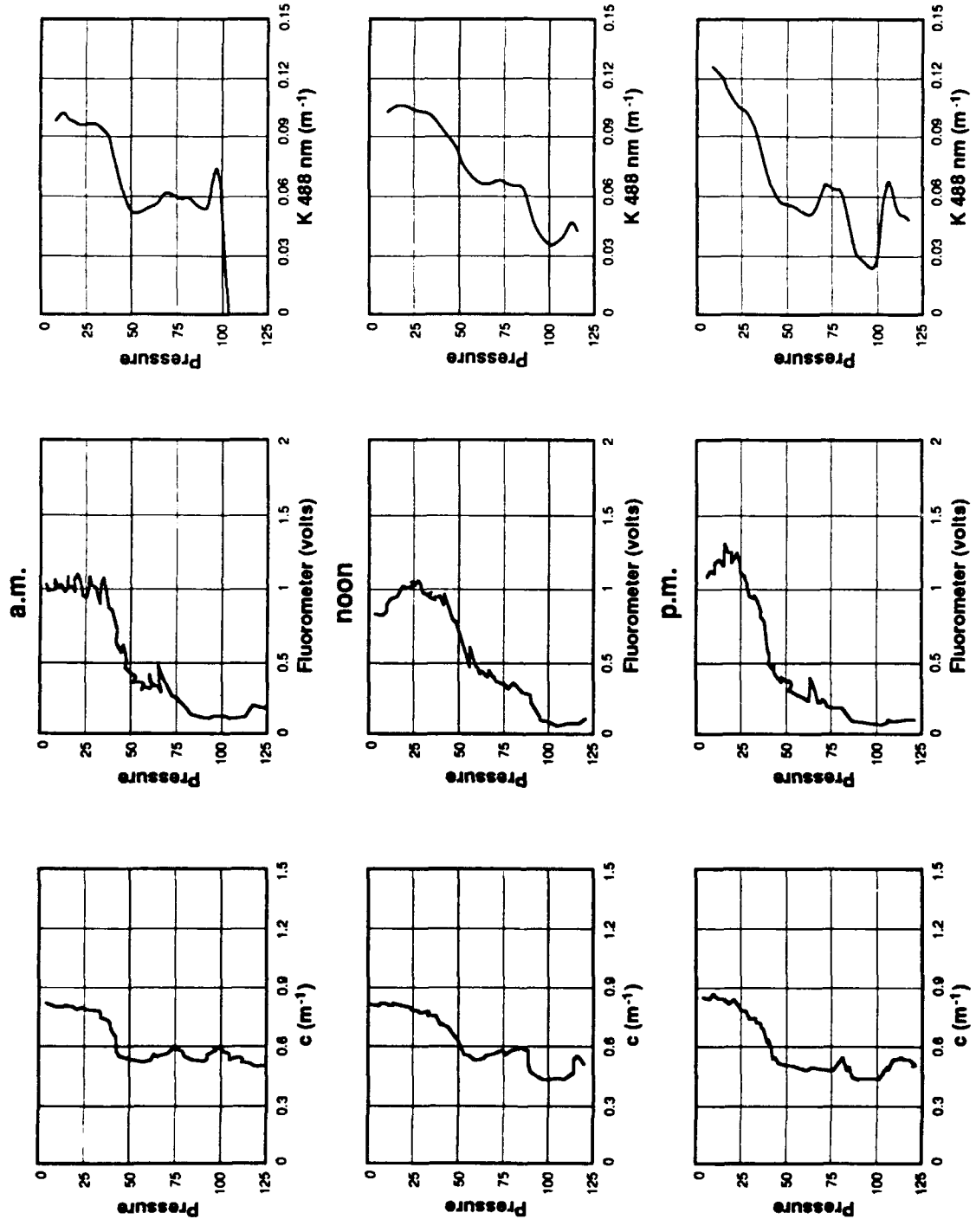


**Figure 8. Representative profiles taken from the a.m., noon, and p.m. sampling periods for Station 8. C is the beam attenuation coefficient with units of $m^{-1}$, the fluorometer measurement is relative and is in volts, and K 488 is the attenuation coefficient calculated from irradiance profiles and also has units of $m^{-1}$.**

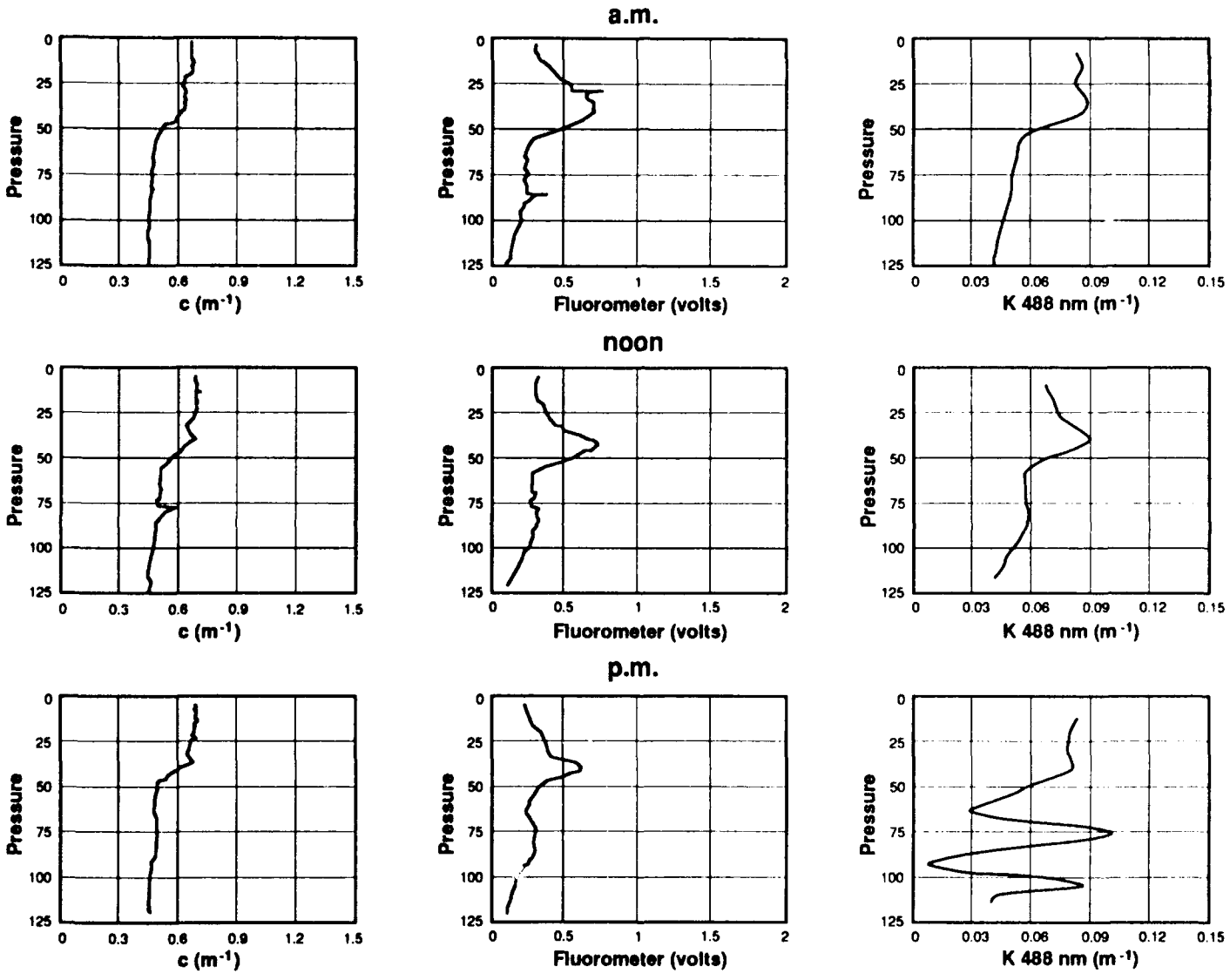


**Figure 9. Representative profiles taken from the a.m., noon, and p.m. sampling periods for Station 9. C is the beam attenuation coefficient with units of $m^{-1}$, the fluorometer measurement is relative and is in volts, and K 488 is the attenuation coefficient calculated from irradiance profiles and also has units of $m^{-1}$.**

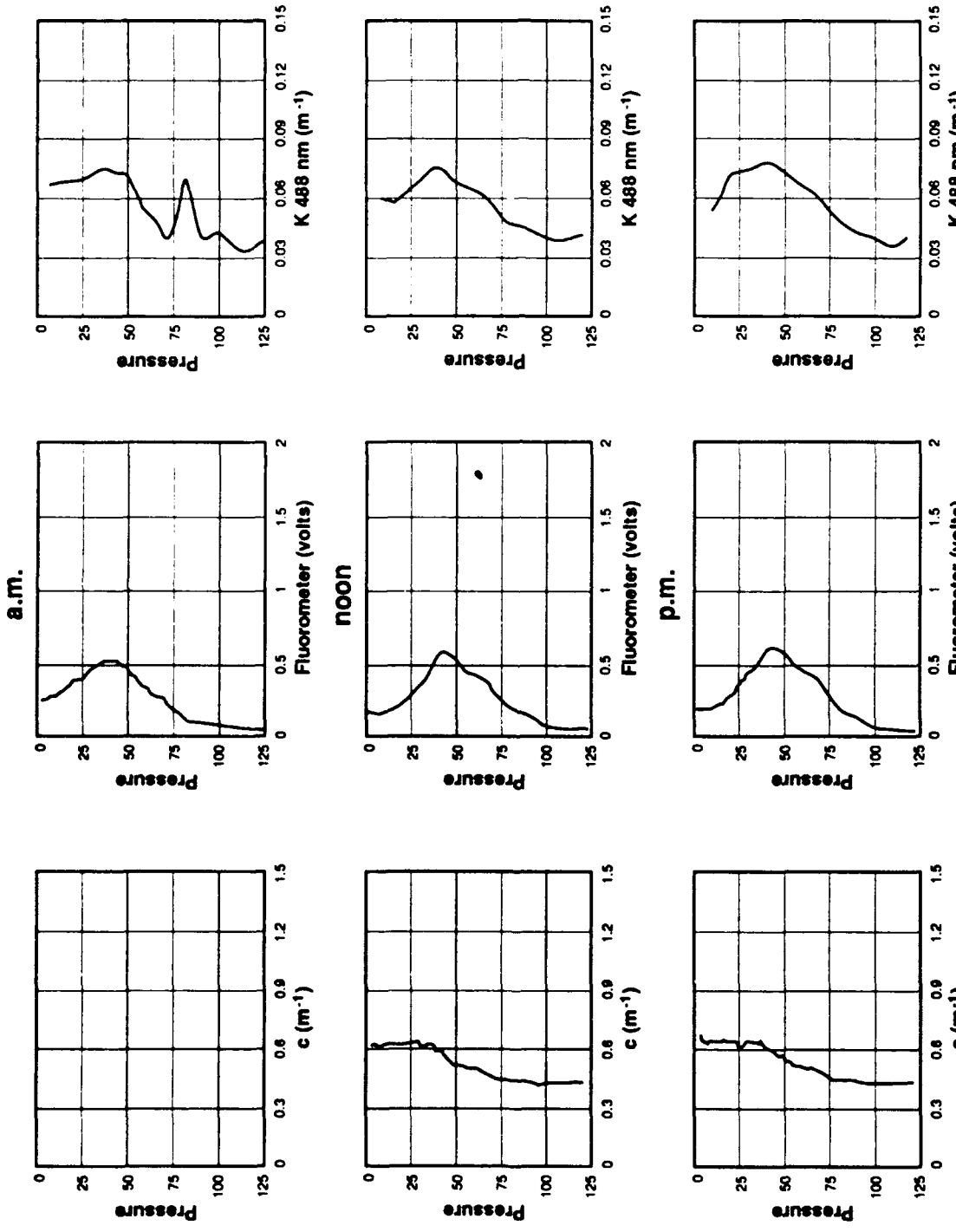


**Figure 10. Representative profiles taken from the a.m., noon, and p.m. sampling periods for Station 10. C is the beam attenuation coefficient with units of $m^{-1}$, the fluorometer measurement is relative and is in volts, and K 488 is the attenuation coefficient calculated from irradiance profiles and also has units of $m^{-1}$.**

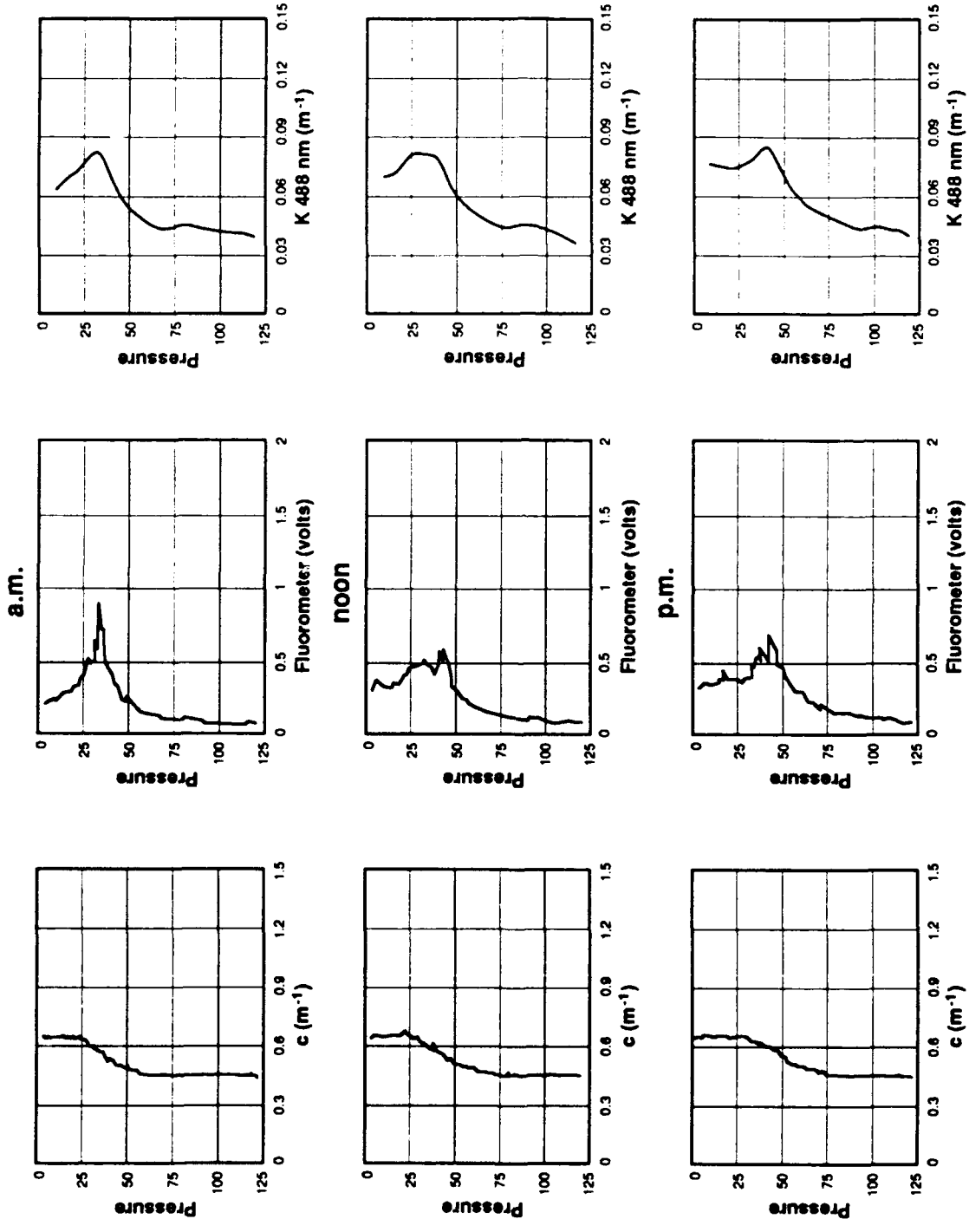


**Figure 11. Representative profiles taken from the a.m., noon, and p.m. sampling periods for Station 11. C is the beam attenuation coefficient with units of $m^{-1}$, the fluorometer measurement is relative and is in volts, and K 488 is the attenuation coefficient calculated from irradiance profiles and also has units of $m^{-1}$.**

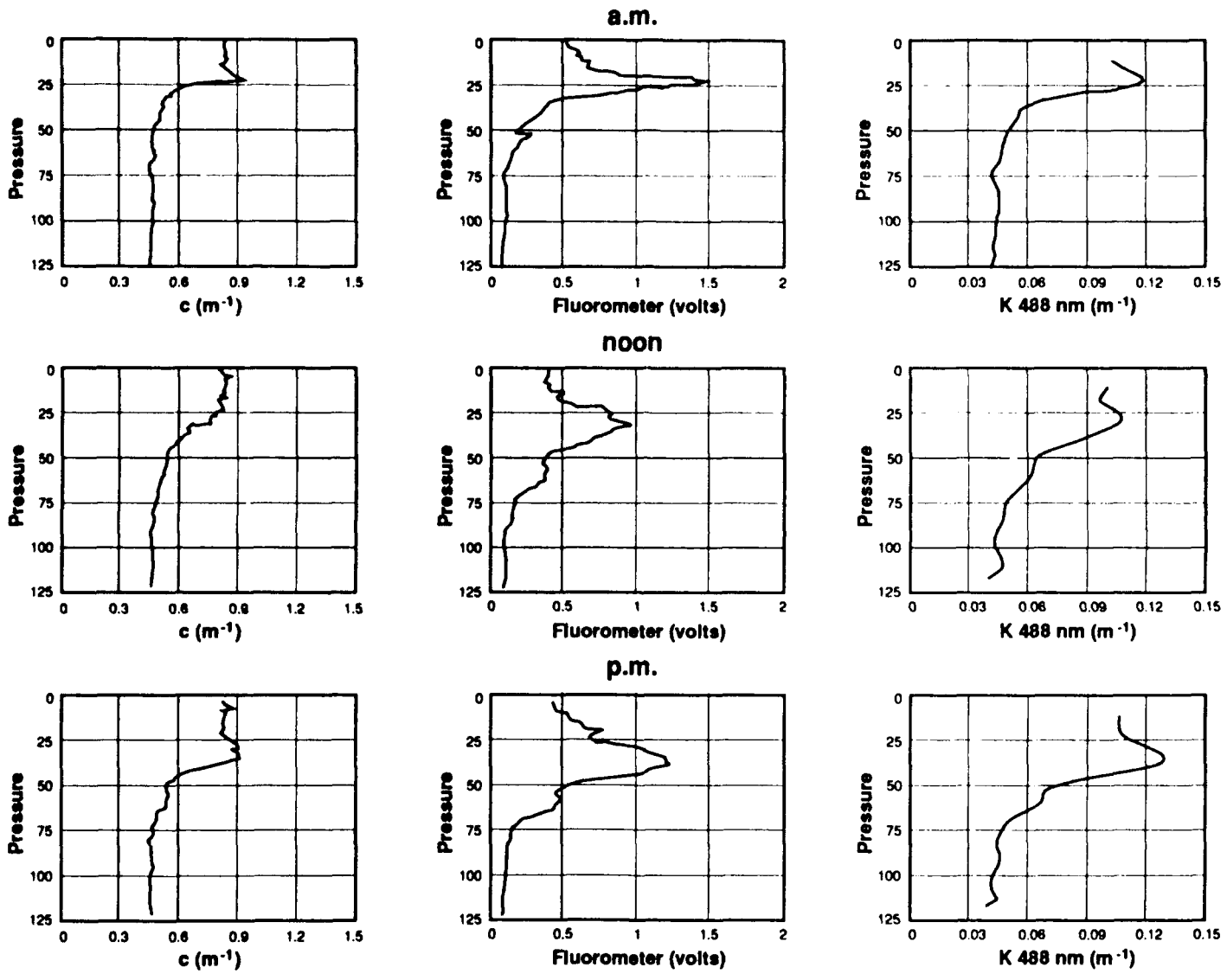


**Figure 12. Representative profiles taken from the a.m., noon, and p.m. sampling periods for Station 12, April 13. C is the beam attenuation coefficient with units of $m^{-1}$, the fluorometer measurement is relative and is in volts, and K 488 is the attenuation coefficient calculated from irradiance profiles and also has units of $m^{-1}$.**

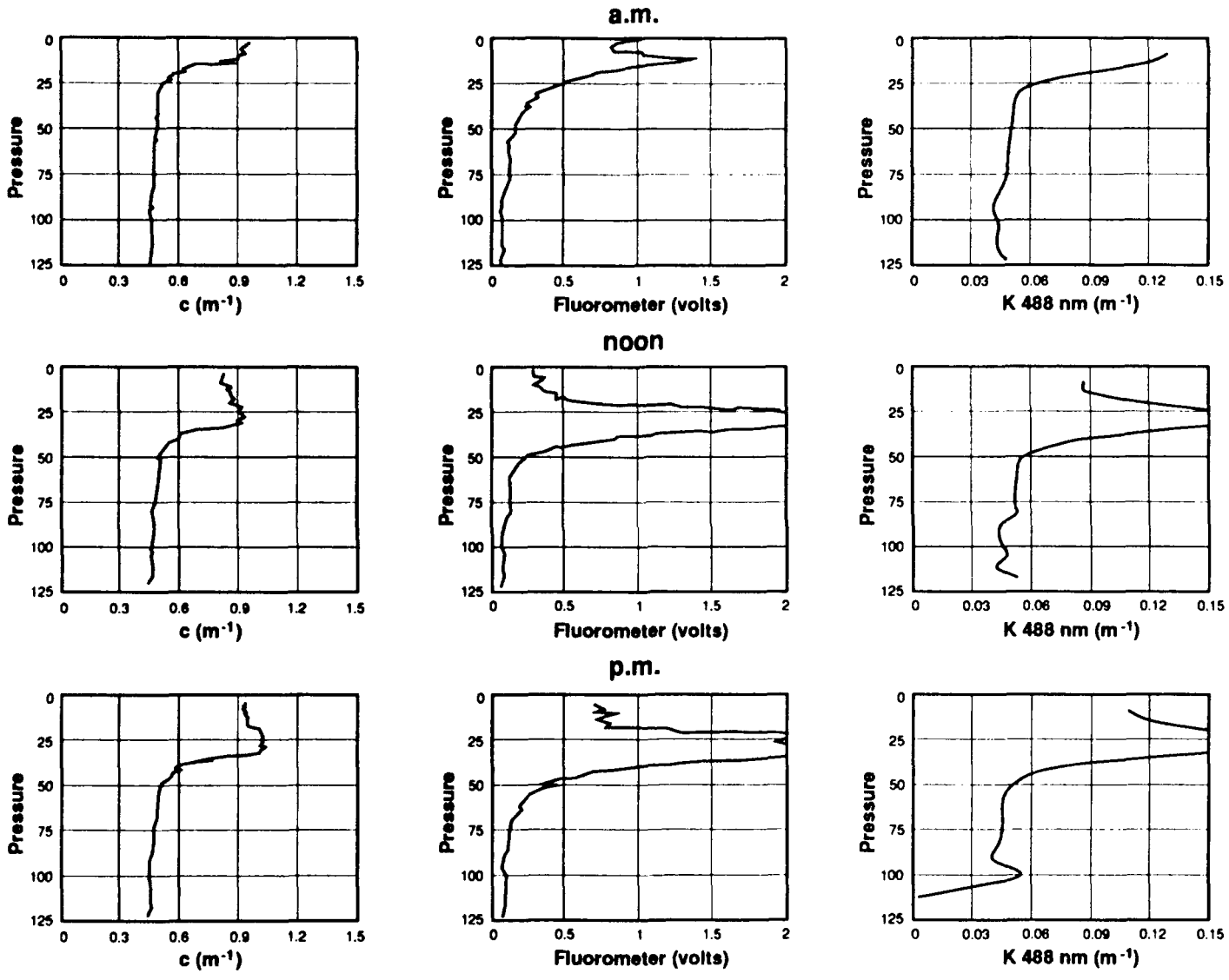


**Figure 13. Representative profiles taken from the a.m., noon, and p.m. sampling periods for Station 12, April 14. C is the beam attenuation coefficient with units of $m^{-1}$, the fluorometer measurement is relative and is in volts, and K 488 is the attenuation coefficient calculated from irradiance profiles and also has units of $m^{-1}$.**

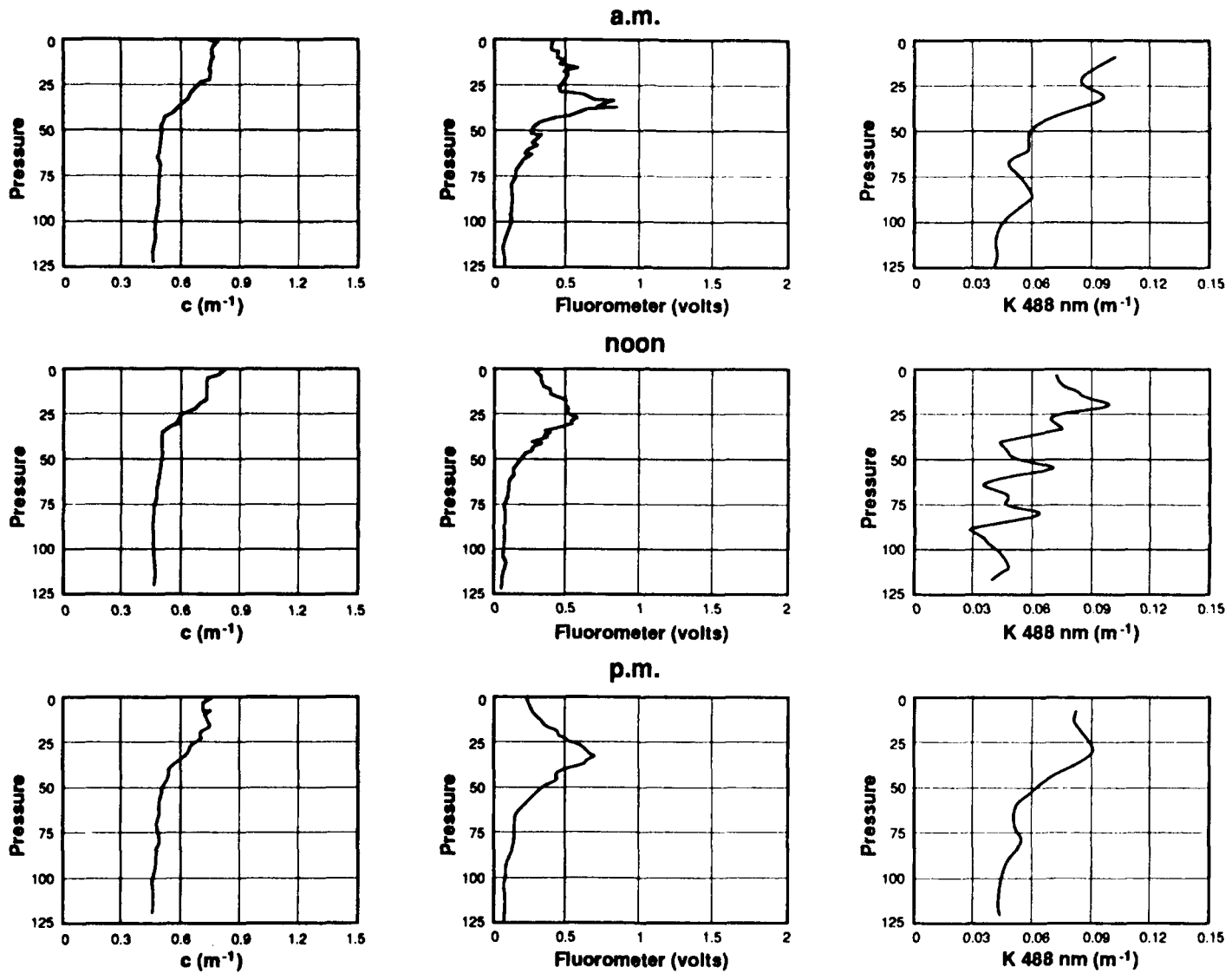


**Figure 14. Representative profiles taken from the a.m., noon, and p.m. sampling periods for Station 12, April 15. C is the beam attenuation coefficient with units of $m^{-1}$, the fluorometer measurement is relative and is in volts, and K 488 is the attenuation coefficient calculated from irradiance profiles and also has units of $m^{-1}$.**

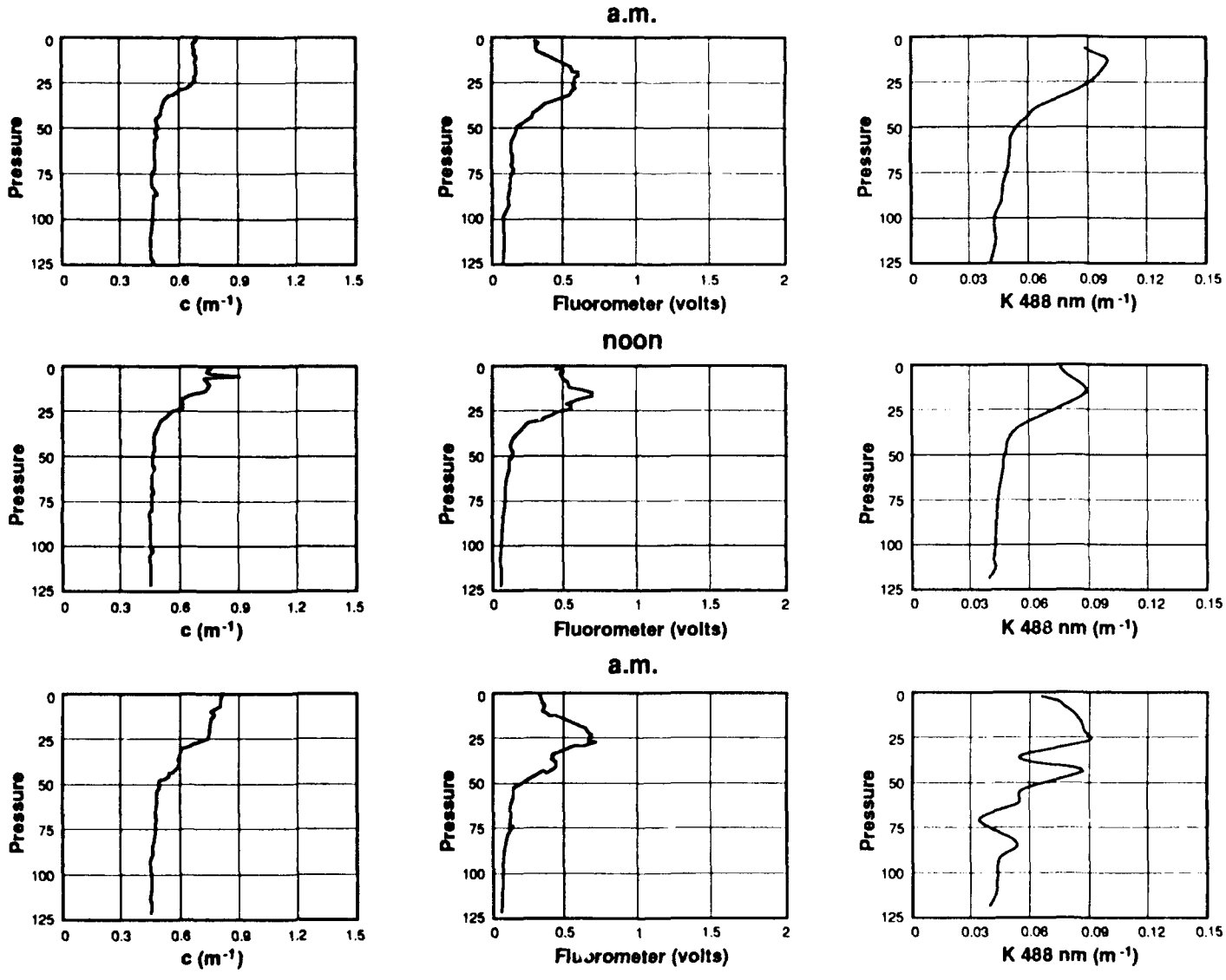


**Figure 15. Representative profiles taken from the a.m., noon, and p.m. sampling periods for Station 12, April 16. C is the beam attenuation coefficient with units of $m^{-1}$, the fluorometer measurement is relative and is in volts, and K 488 is the attenuation coefficient calculated from irradiance profiles and also has units of $m^{-1}$.**

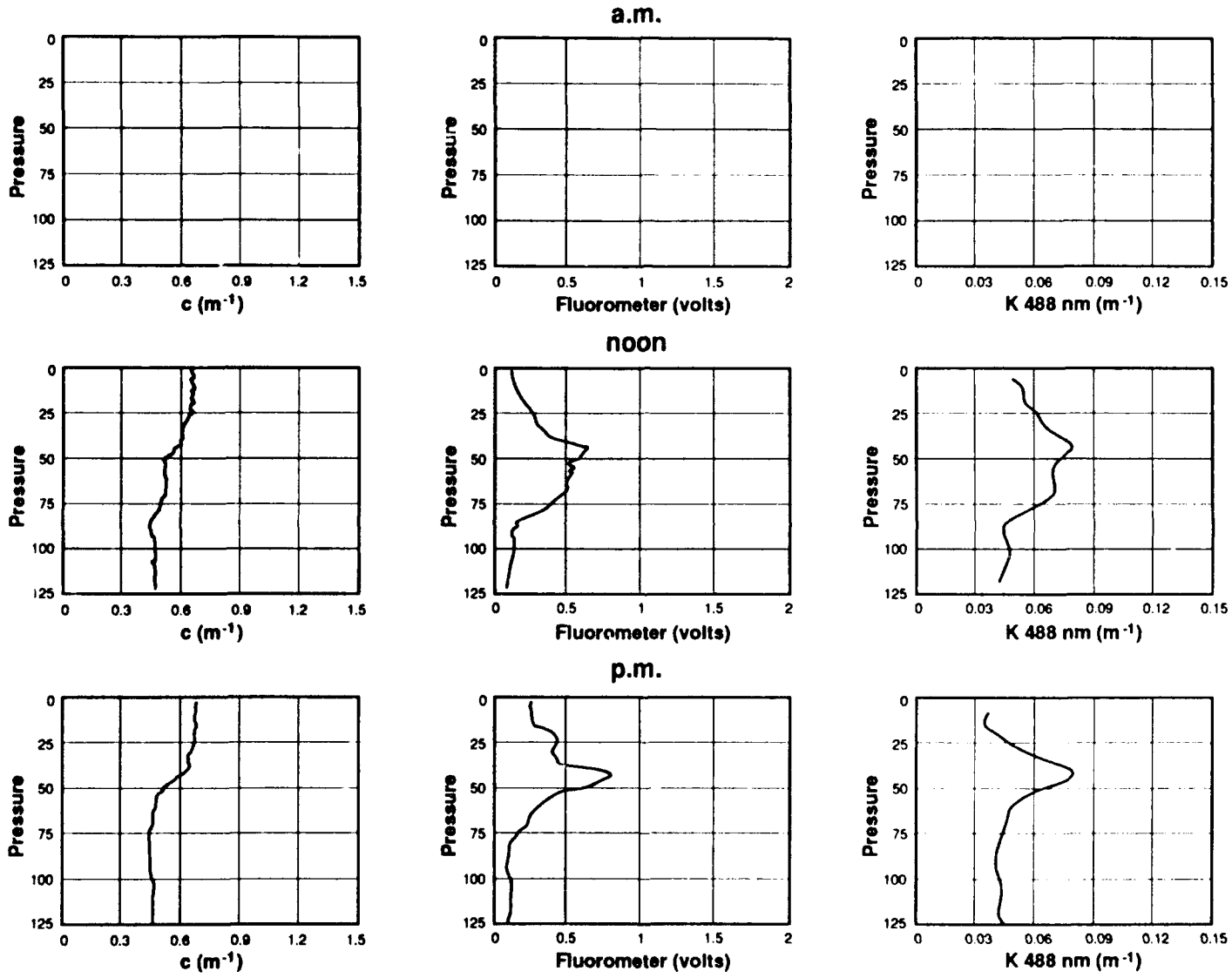


**Figure 16. Representative profiles taken from the a.m., noon, and p.m. sampling periods for Station 13. C is the beam attenuation coefficient with units of $m^{-1}$, the fluorometer measurement is relative and is in volts, and K 488 is the attenuation coefficient calculated from irradiance profiles and also has units of $m^{-1}$.**

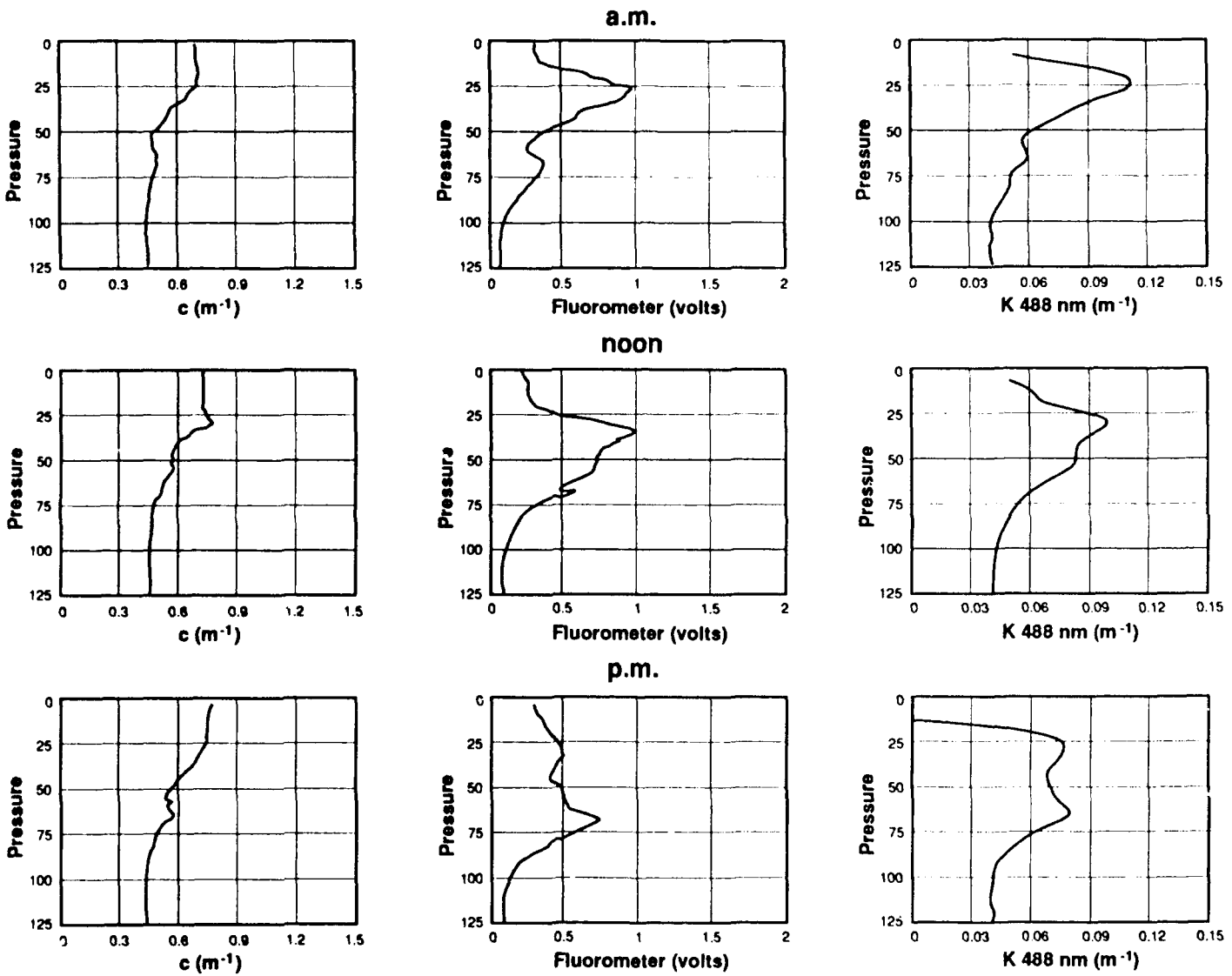


**Figure 17. Representative profiles taken from the a.m., noon, and p.m. sampling periods for Station 14. C is the beam attenuation coefficient with units of $m^{-1}$, the fluorometer measurement is relative and is in volts, and K 488 is the attenuation coefficient calculated from irradiance profiles and also has units of $m^{-1}$.**

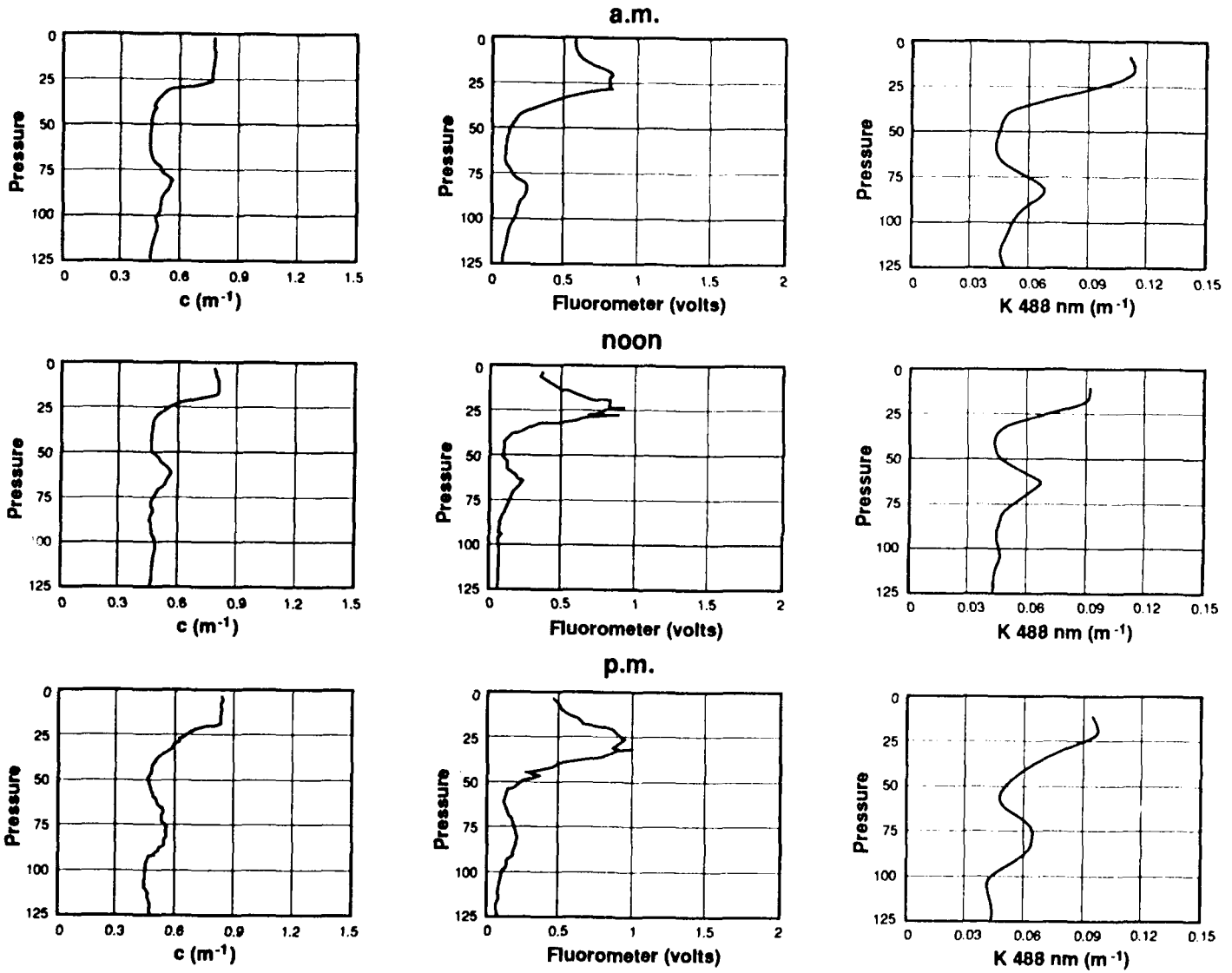


**Figure 18. Representative profiles taken from the a.m., noon, and p.m. sampling periods for Station 15. C is the beam attenuation coefficient with units of $m^{-1}$, the fluorometer measurement is relative and is in volts, and K 488 is the attenuation coefficient calculated from irradiance profiles and also has units of $m^{-1}$.**

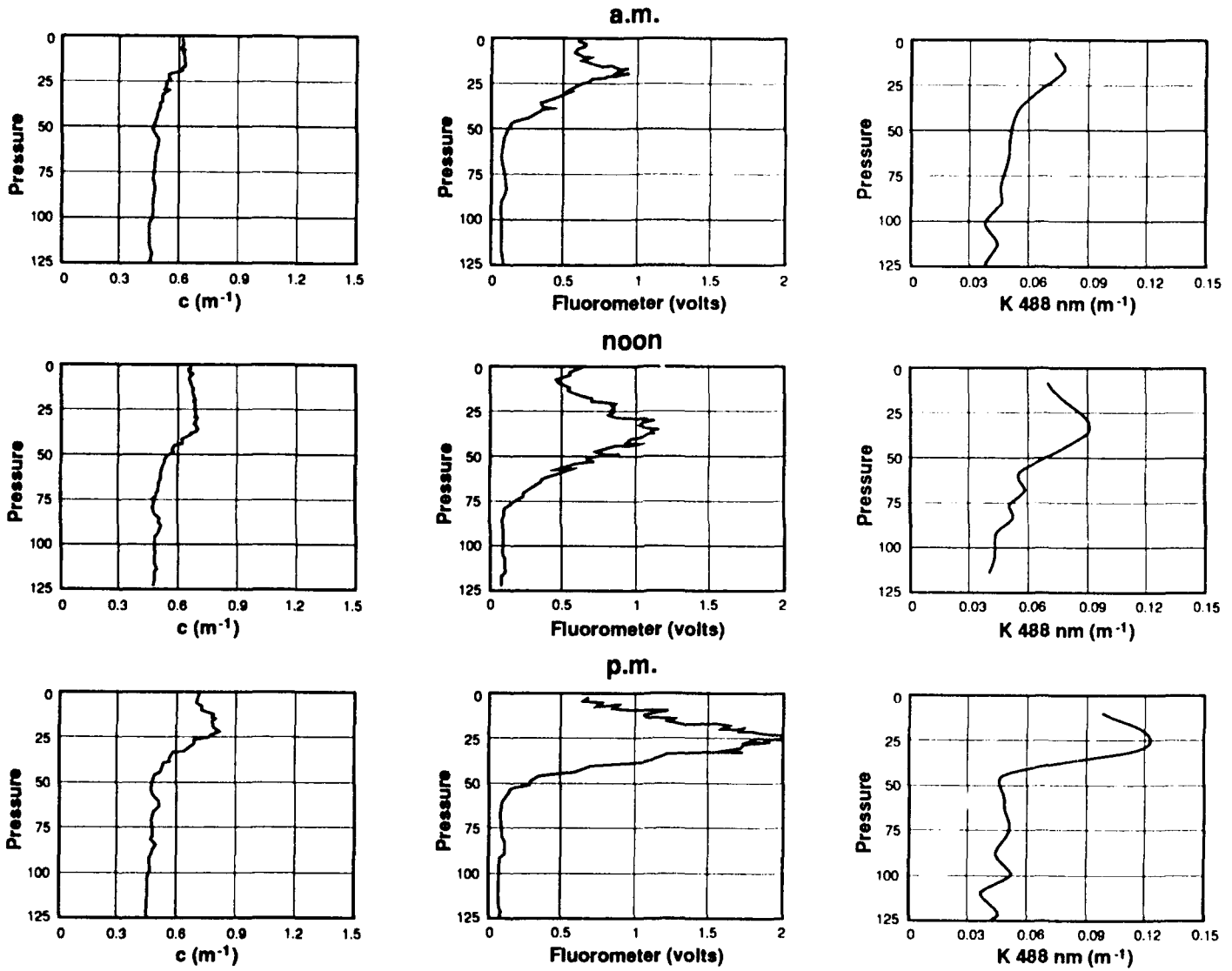


**Figure 19. Representative profiles taken from the a.m., noon, and p.m. sampling periods for Station 16. C is the beam attenuation coefficient with units of $m^{-1}$, the fluorometer measurement is relative and is in volts, and K 488 is the attenuation coefficient calculated from irradiance profiles and also has units of $m^{-1}$.**

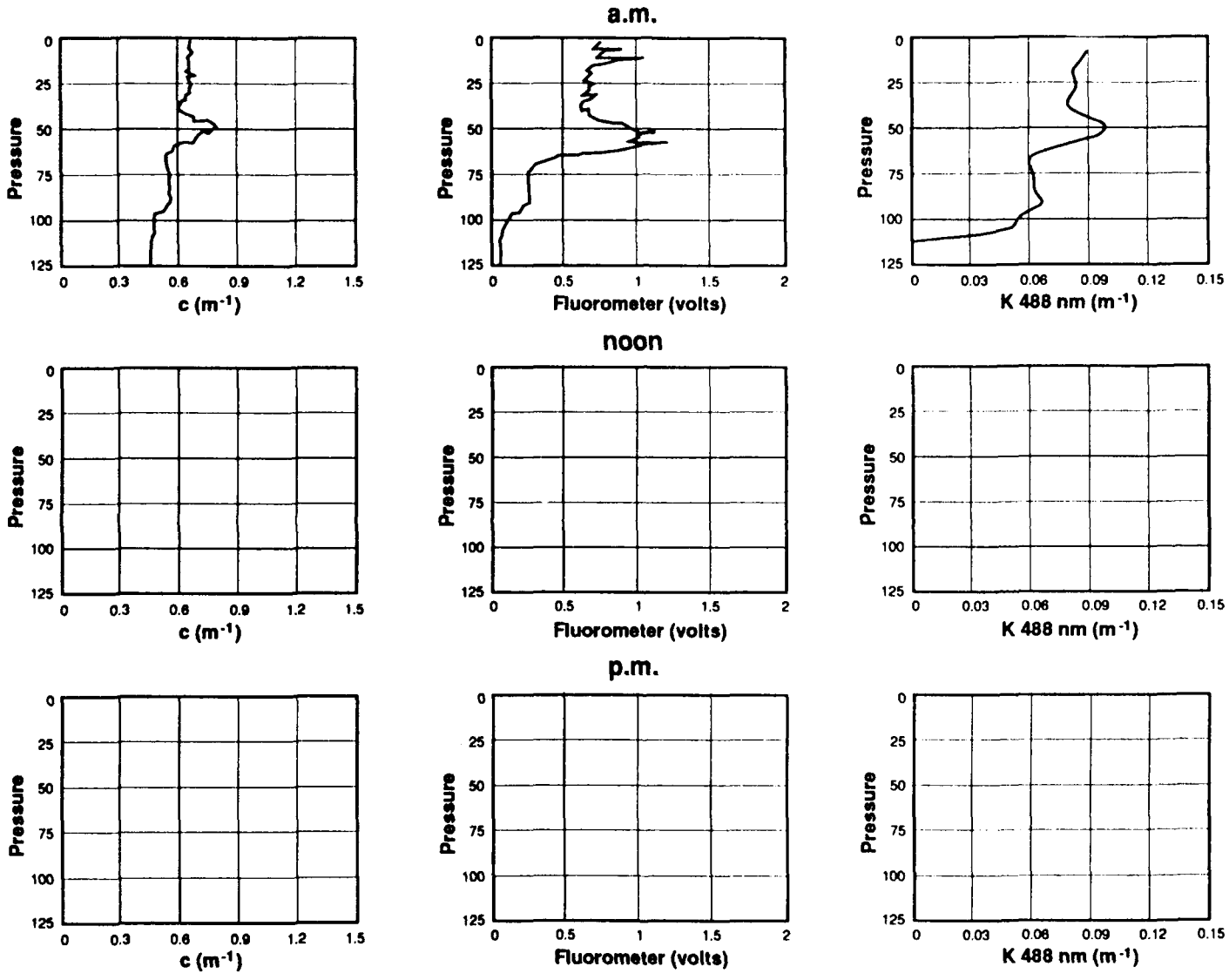


**Figure 20. Representative profiles taken from the a.m., noon, and p.m. sampling periods for Station 17. C is the beam attenuation coefficient with units of $m^{-1}$, the fluorometer measurement is relative and is in volts, and K 488 is the attenuation coefficient calculated from irradiance profiles and also has units of $m^{-1}$.**

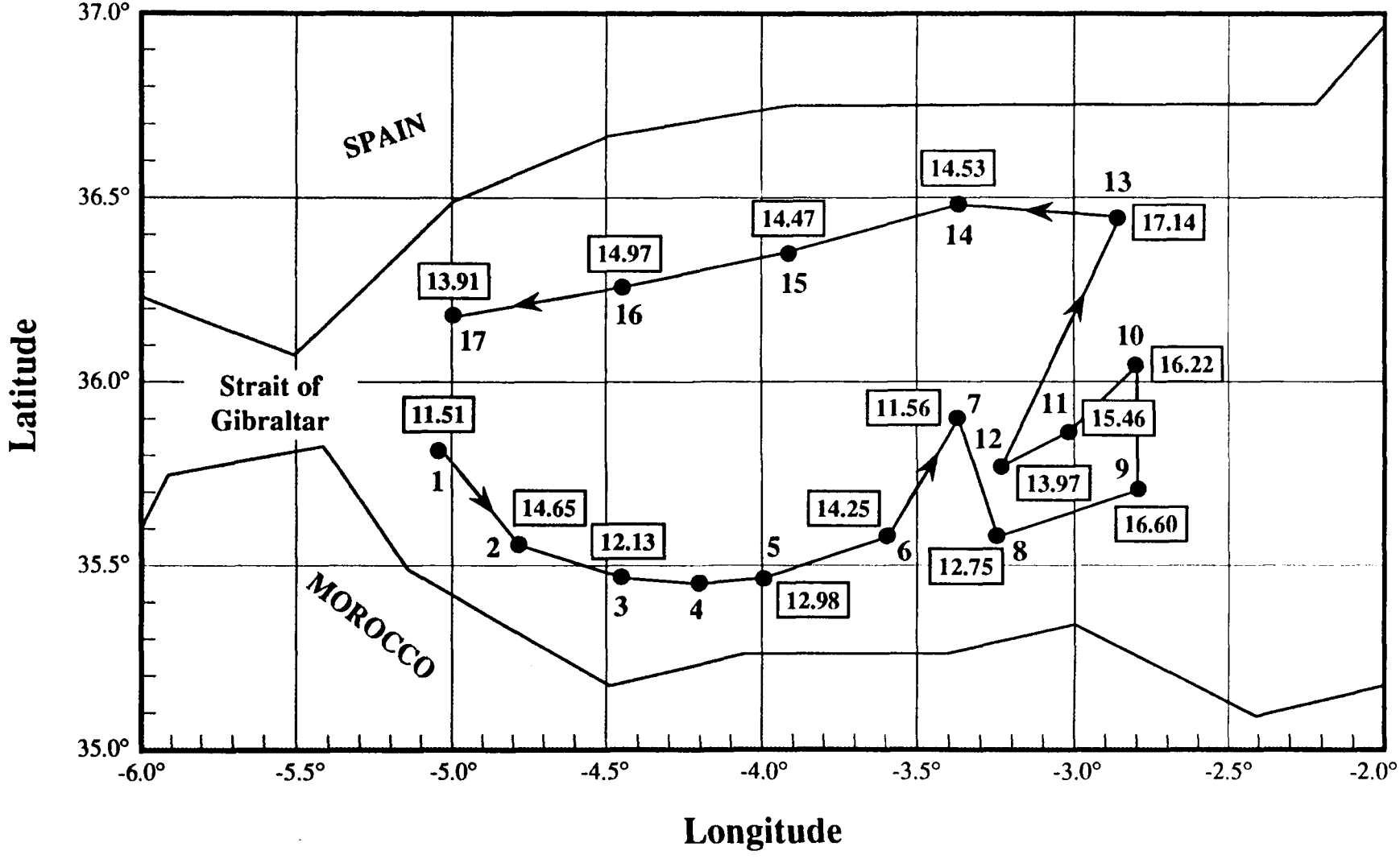


**Figure 21. Station Locations and Cruise 1306-91 Track, Alboran Sea, with Average Attenuation Lengths (m) in boxes for each station. (For Example, Representative Attenuation Length in Sargasso Sea = 32 m.)**

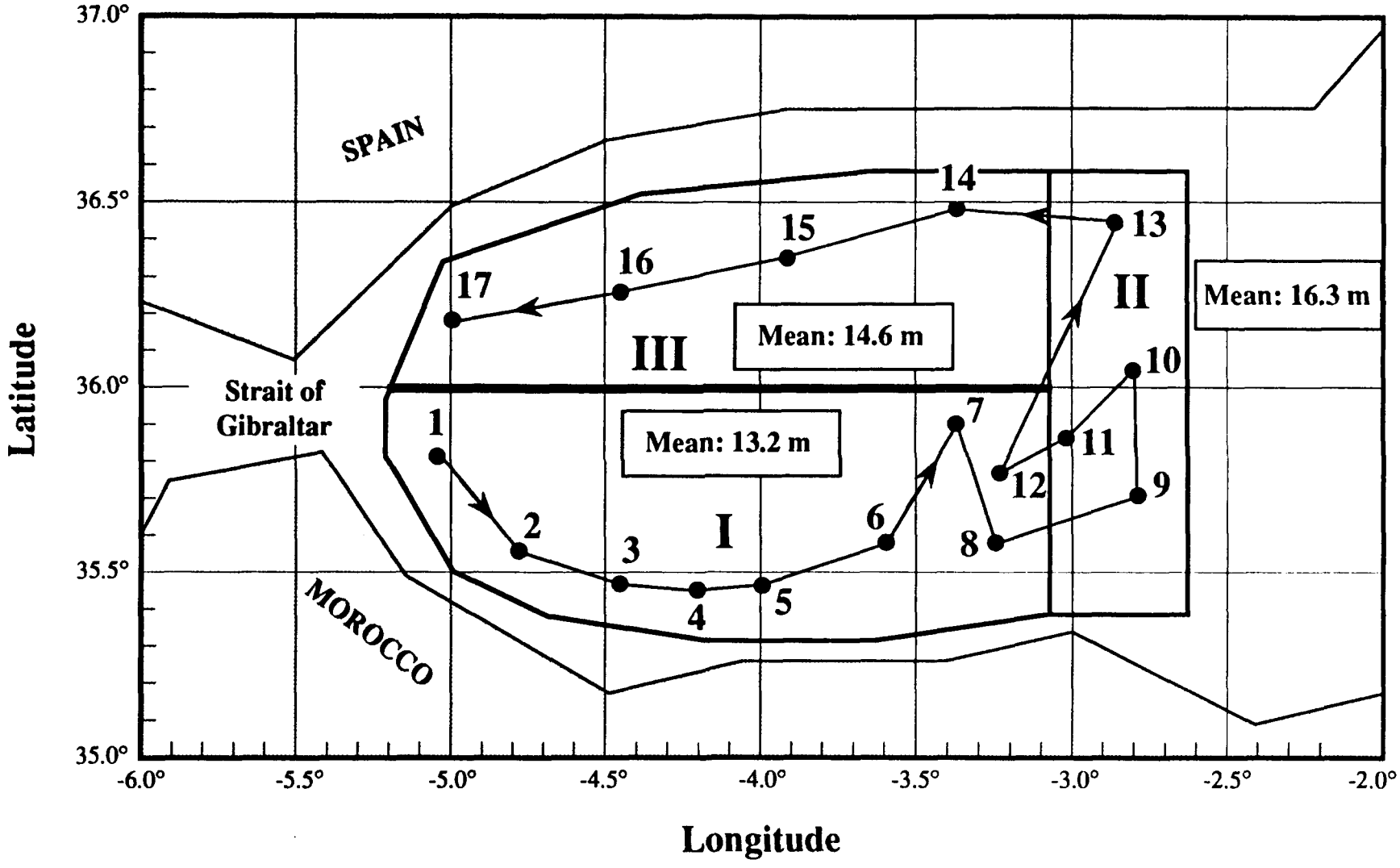


**Figure 22. Alboran Sea Provinces as determined by Attenuation Length. (Province I and II Significantly Different at 0.2%, Province I and III Significantly Different at 0.2%, and Province II and III Significantly Different at 1.0%.)**

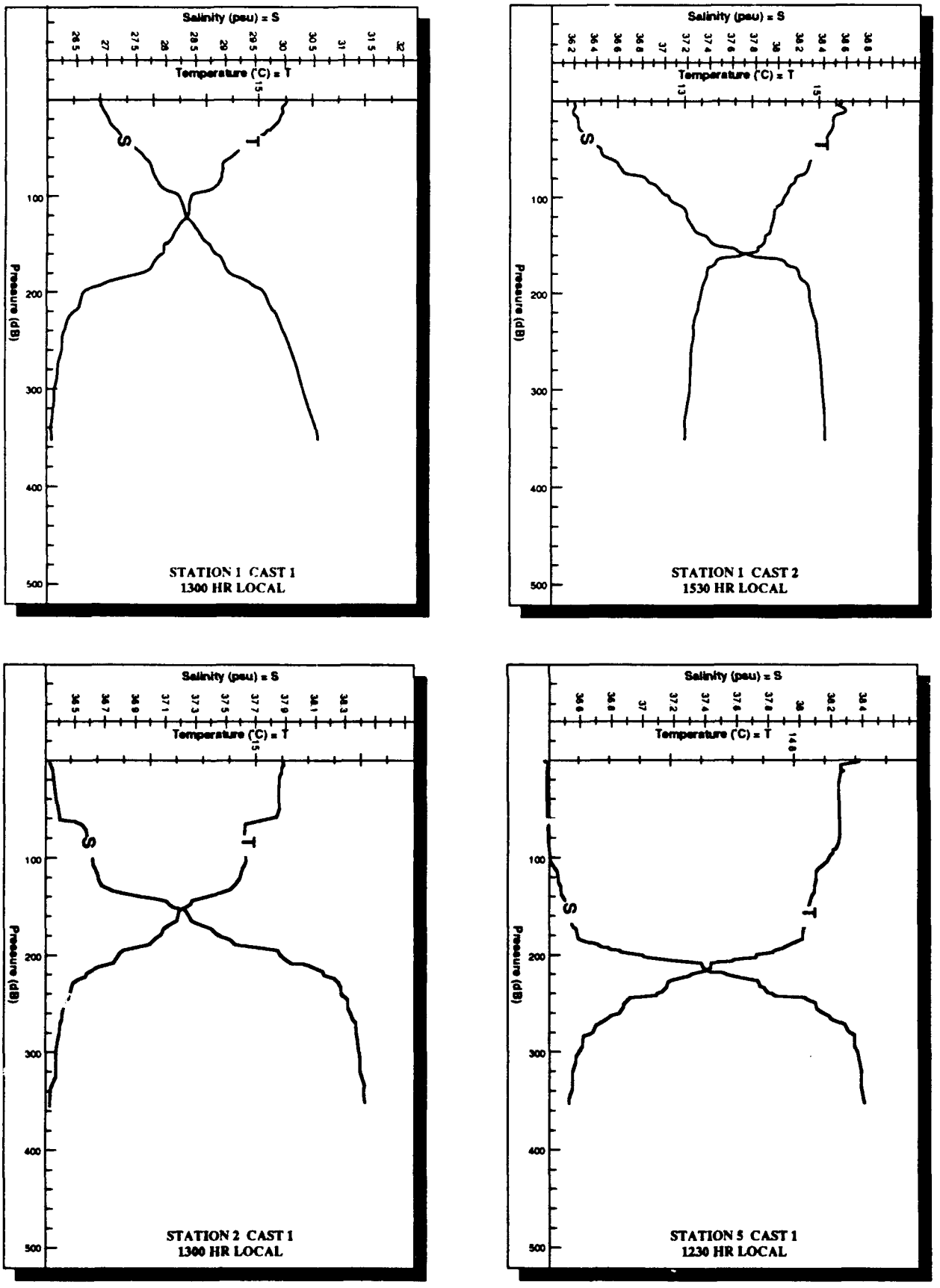


**Figure 23. Temperature and salinity profiles as obtained from CTD casts for Station 1 (casts at 1300 and 1530 hr local), Station 2 (cast at 1300 hr local), and Station 5 (cast at 1230 hr local).**

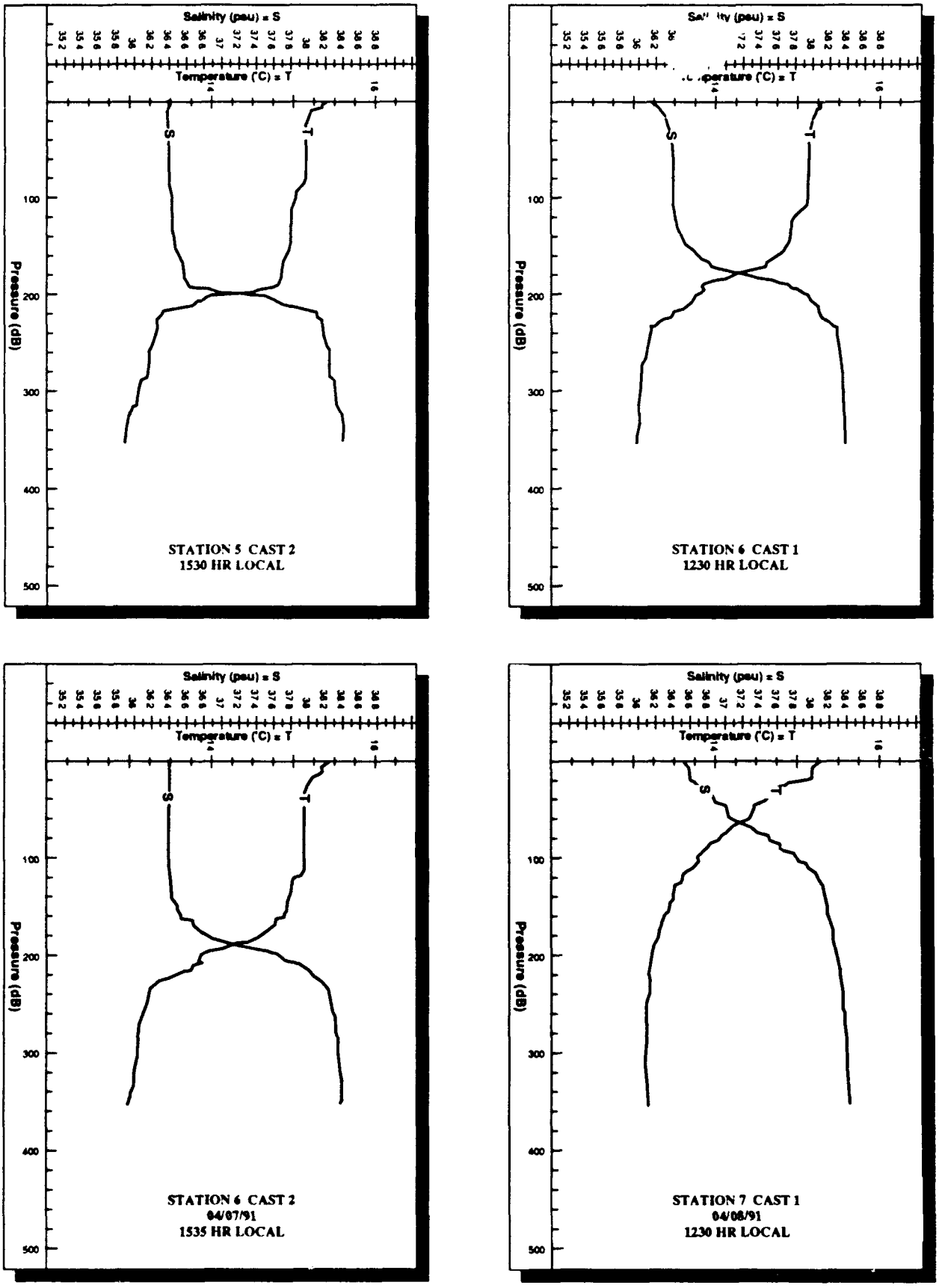


**Figure 24. Temperature and salinity profiles as obtained from CTD casts for Station 5 (cast at 1530 hr local), Station 6 (casts at 1230 and 1535 hr local), and Station 7 (cast at 1230 hr local).**

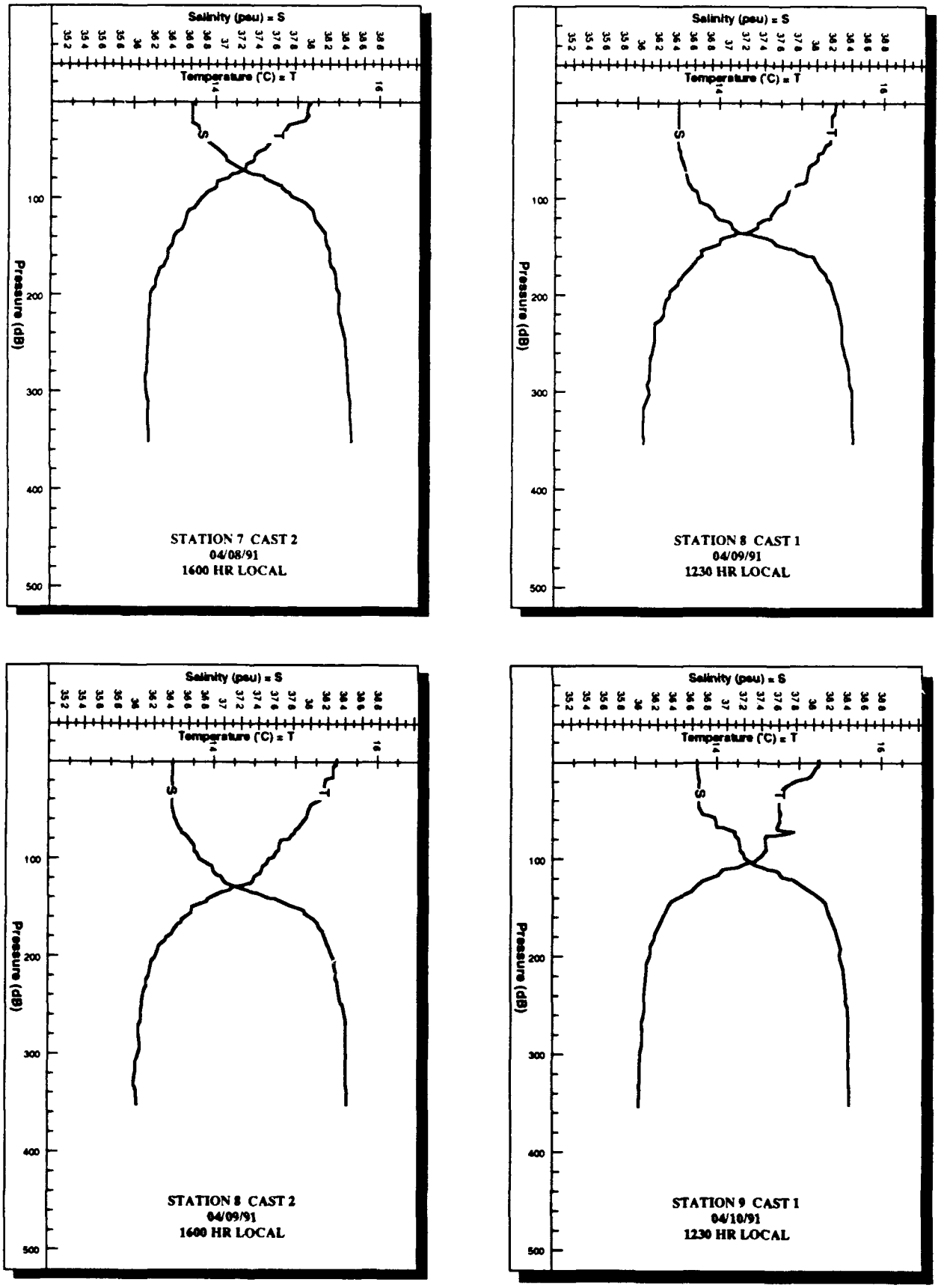


**Figure 25. Temperature and salinity profiles as obtained from CTD casts for Station 7 (cast at 1600 hr local), Station 8 (casts at 1230 and 1600 hr local), and Station 9 (cast at 1230 hr local).**

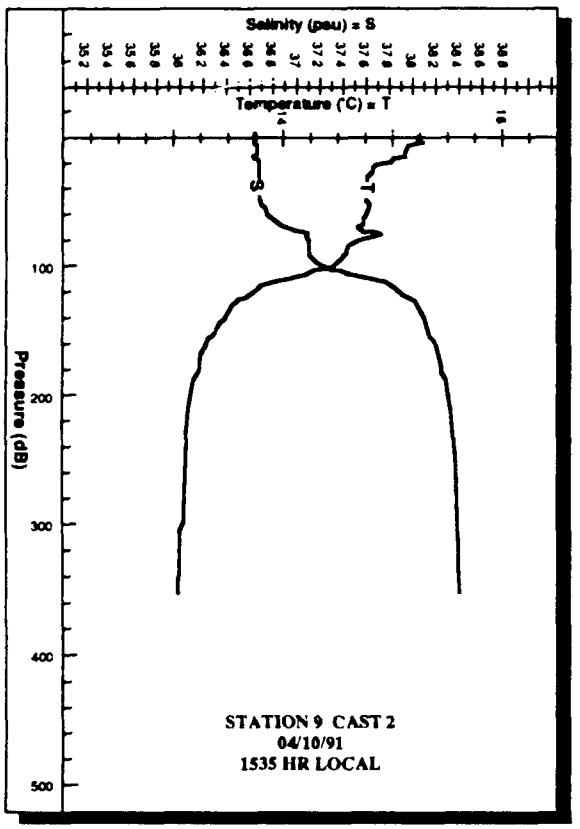


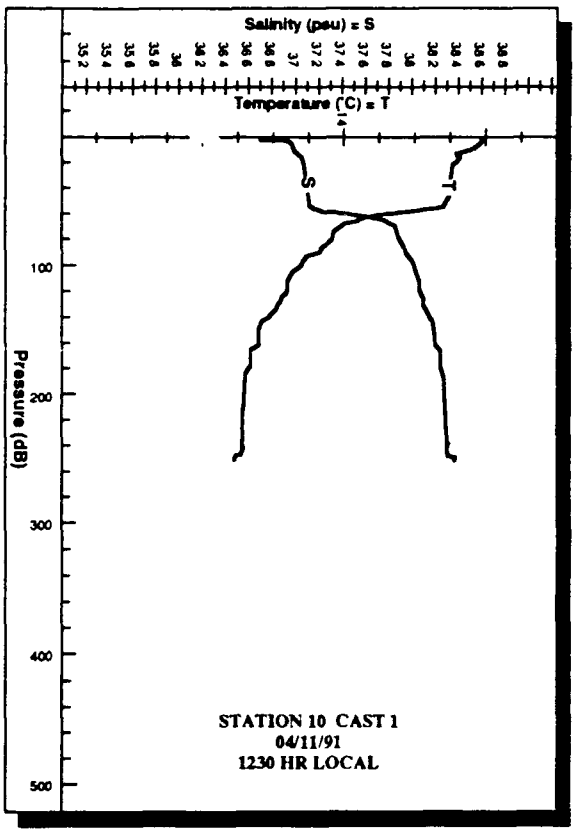


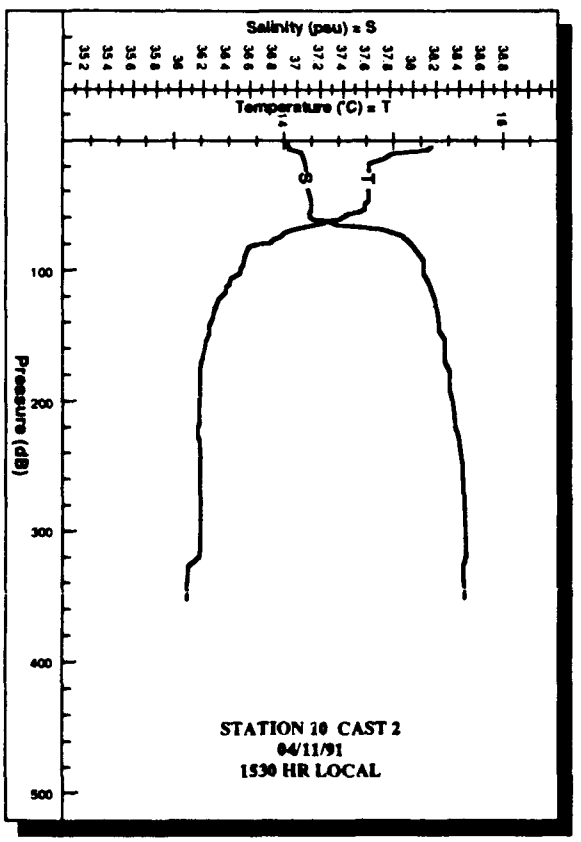


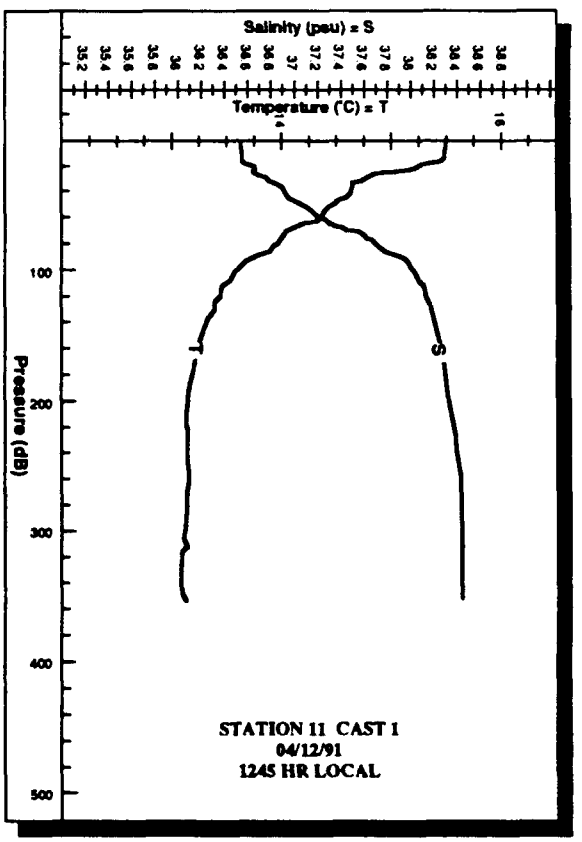


**Figure 26. Temperature and salinity profiles as obtained from CTD casts for Station 9 (cast at 1535 hr local), Station 10 (casts at 1230 and 1530 hr local), and Station 11 (cast at 1245 hr local).**

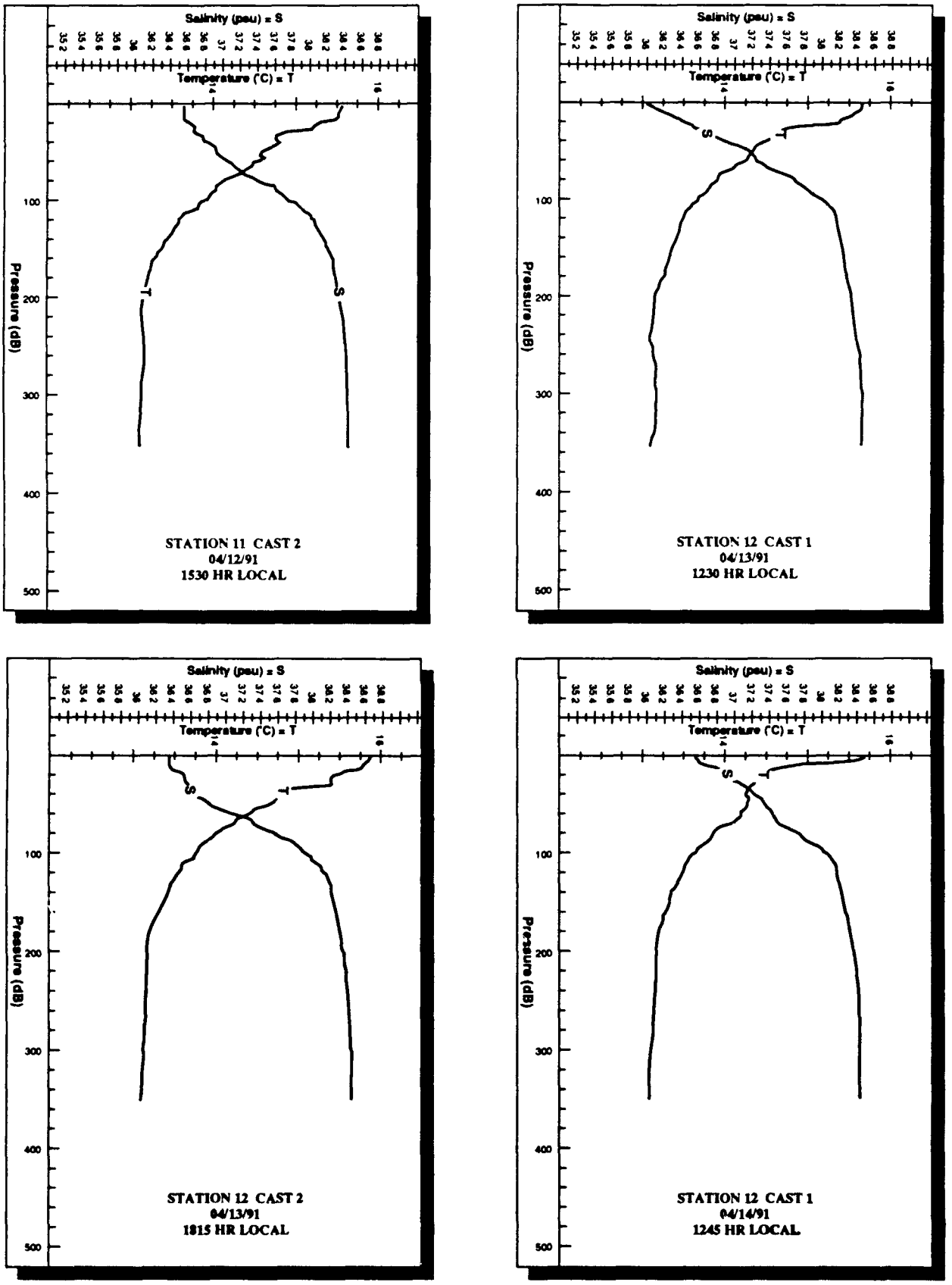


**Figure 27. Temperature and salinity profiles as obtained from CTD casts for Station 11 (cast at 1530 hr local), Station 12 - April 13 (casts at 1230 and 1815 hr local), and Station 12 - April 14 (cast at 1245 hr local).**

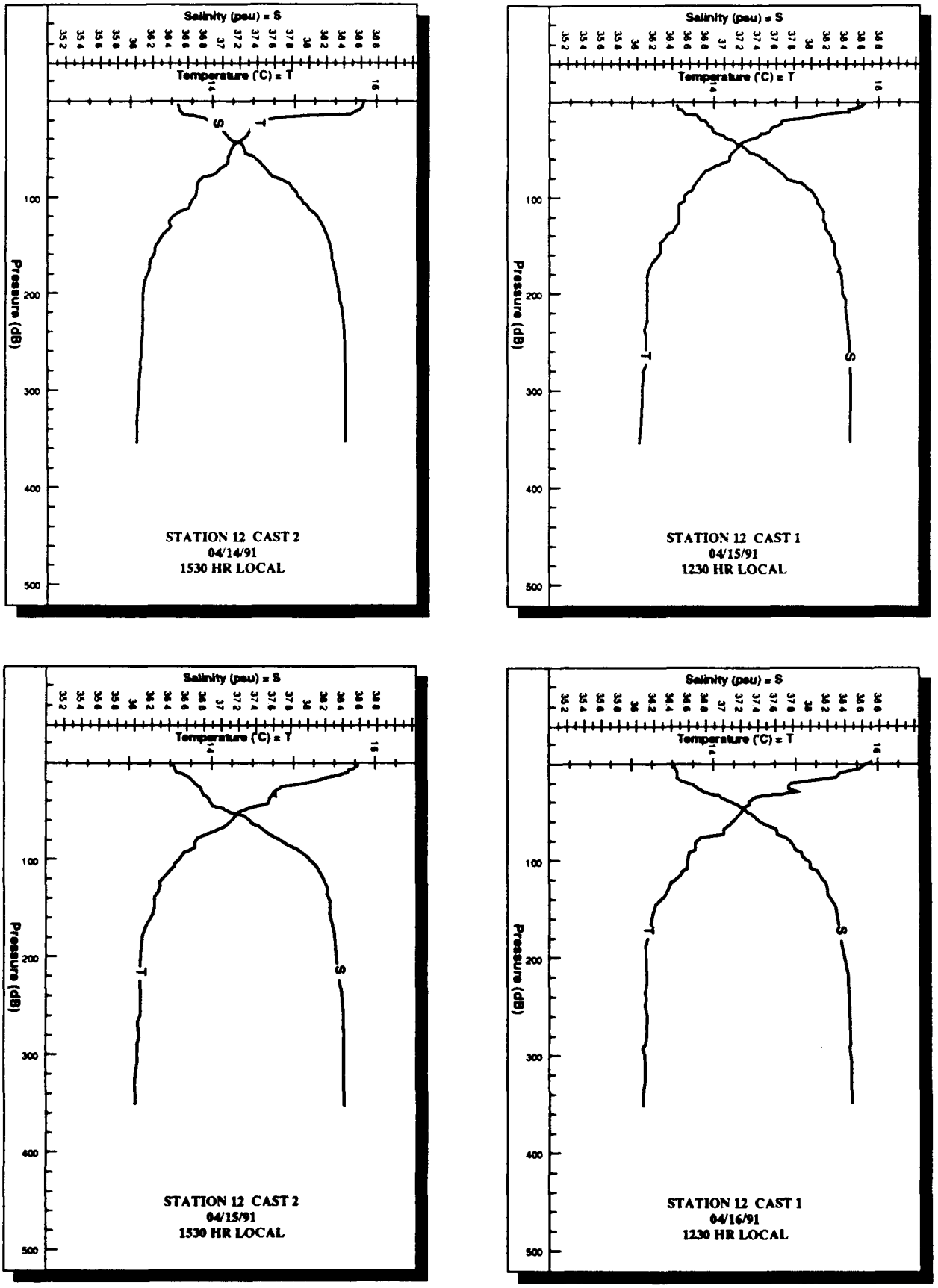


**Figure 28. Temperature and salinity profiles as obtained from CTD casts for Station 12 - April 14 (cast at 1530 hr local), Station 12 - April 15 (casts at 1230 and 1530 hr local), and Station 12 - April 16 (cast at 1230 hr local).**

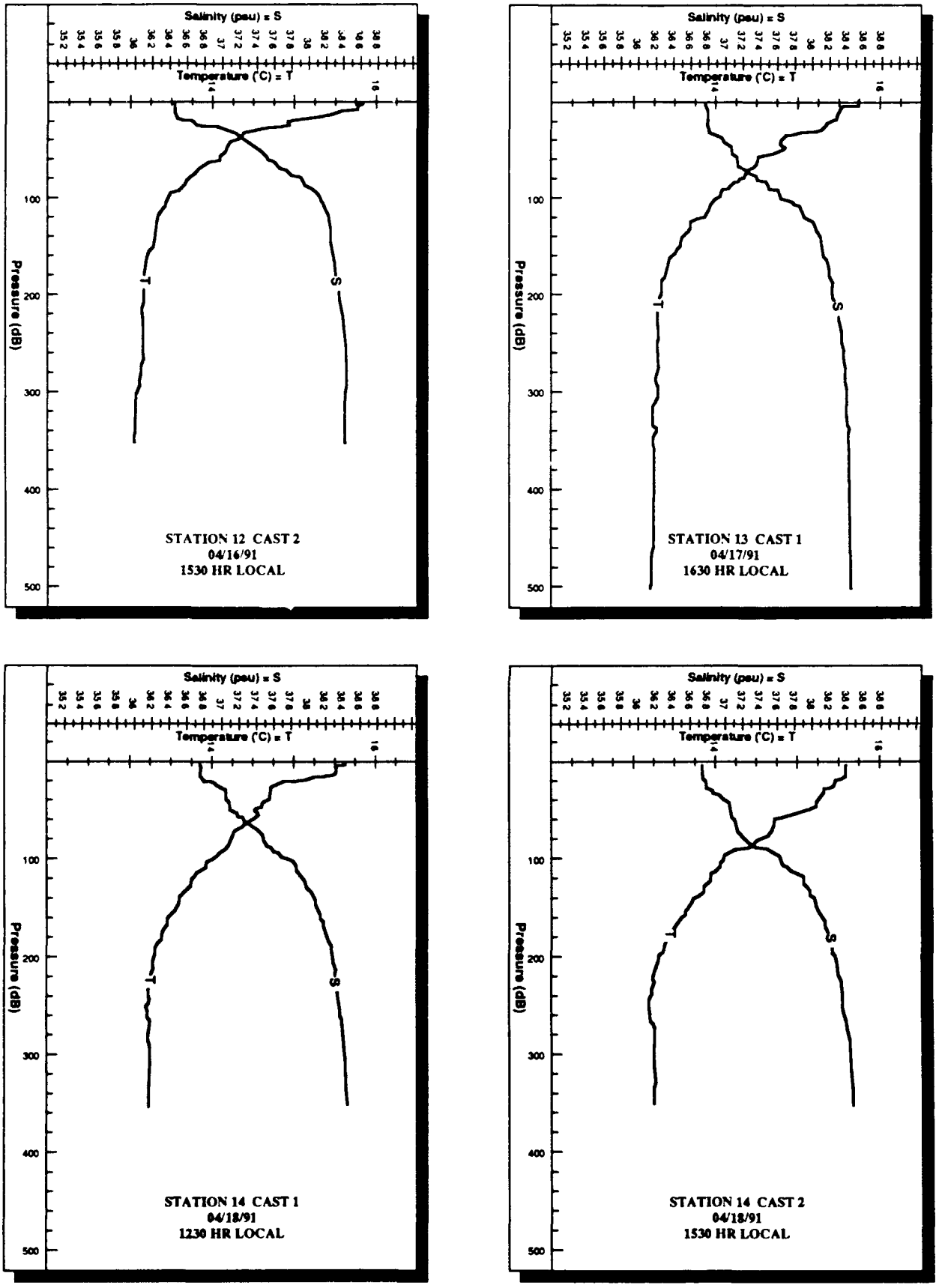


**Figure 29. Temperature and salinity profiles as obtained from CTD casts for Station 12 - April 16 (cast at 1530 hr local), Station 13 (cast at 1630 hr local), and Station 14 (casts at 1230 and 1530 hr local).**

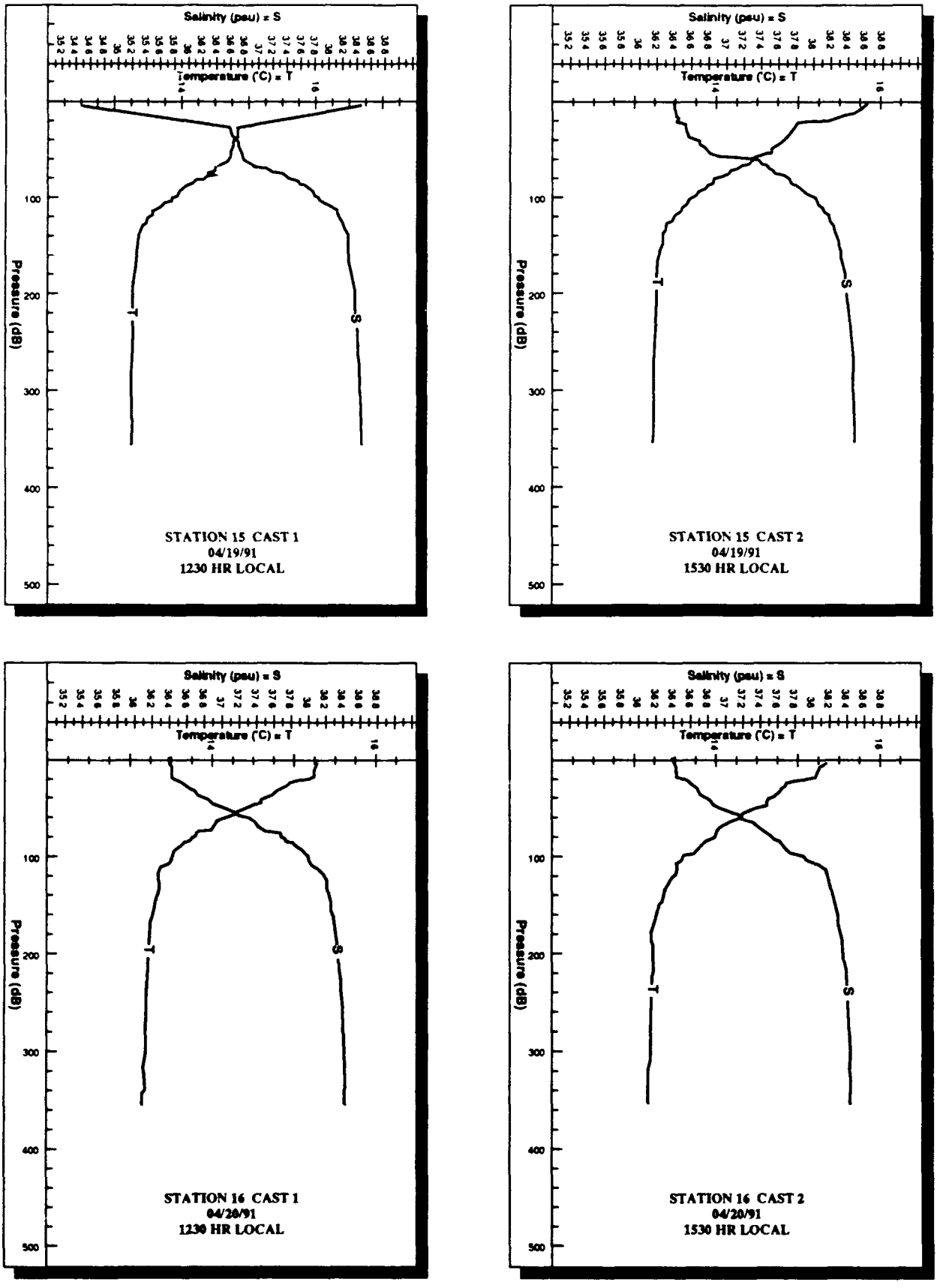


**Figure 30. Temperature and salinity profiles as obtained from CTD casts for Station 15 (casts at 1230 and 1530 hr local), Station 16 (casts at 1230 and 1530 hr local).**

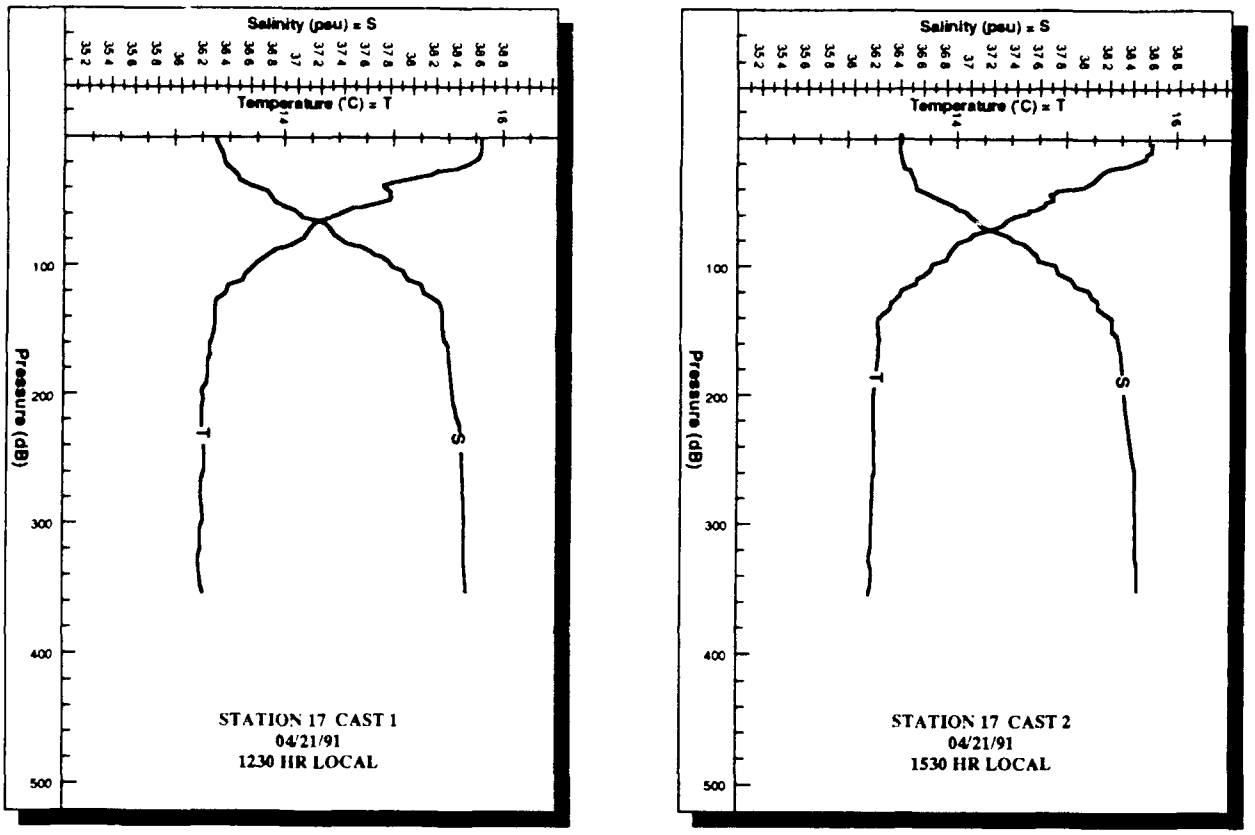


**Figure 31. Temperature and salinity profiles as obtained from CTD casts for Station 17 (casts at 1230 and 1530 hr local).**

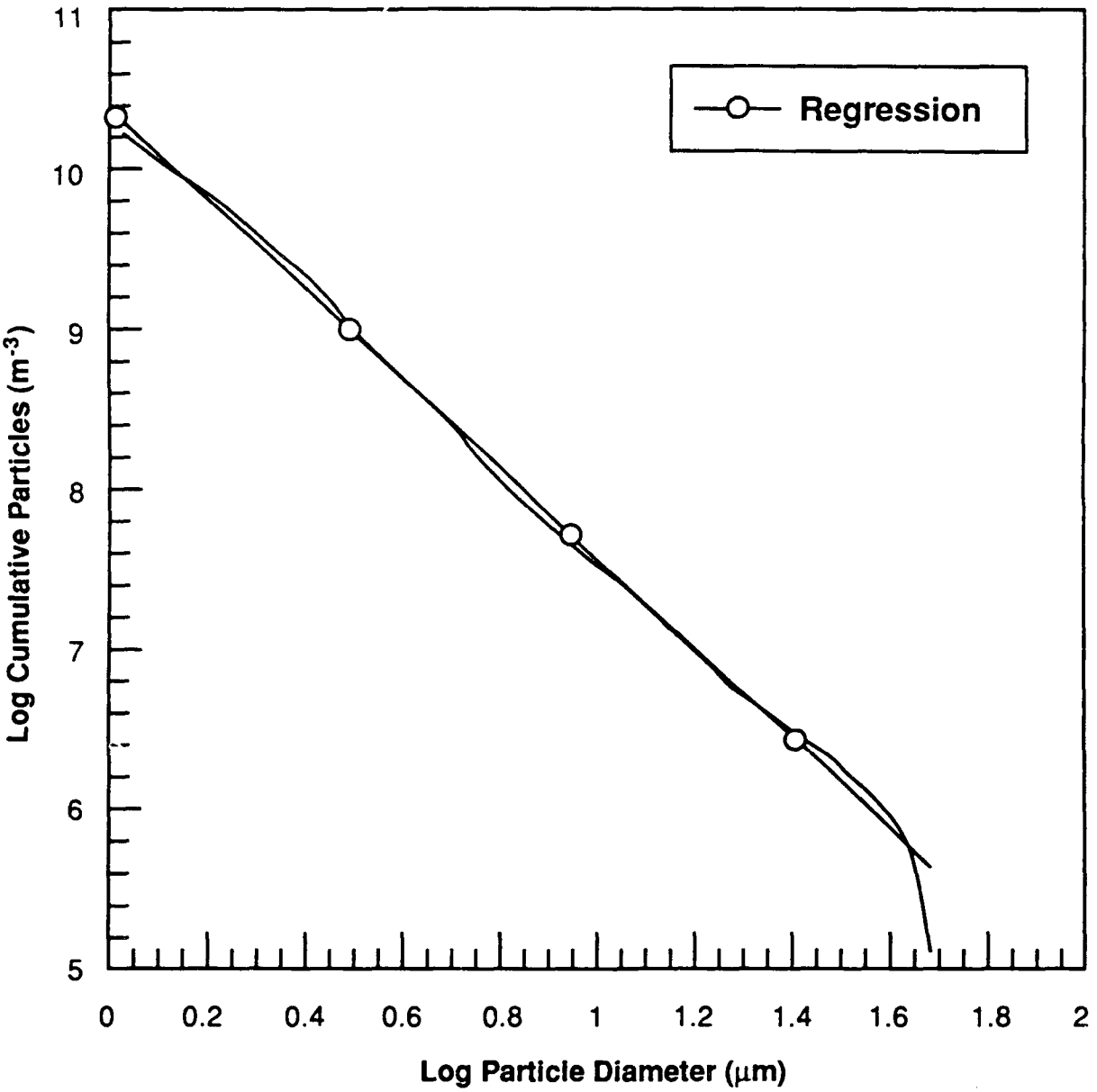


**Figure 32. Log cumulative particle size distribution as a function of the log particle diameter for samples taken at 120 m at Station 10.**

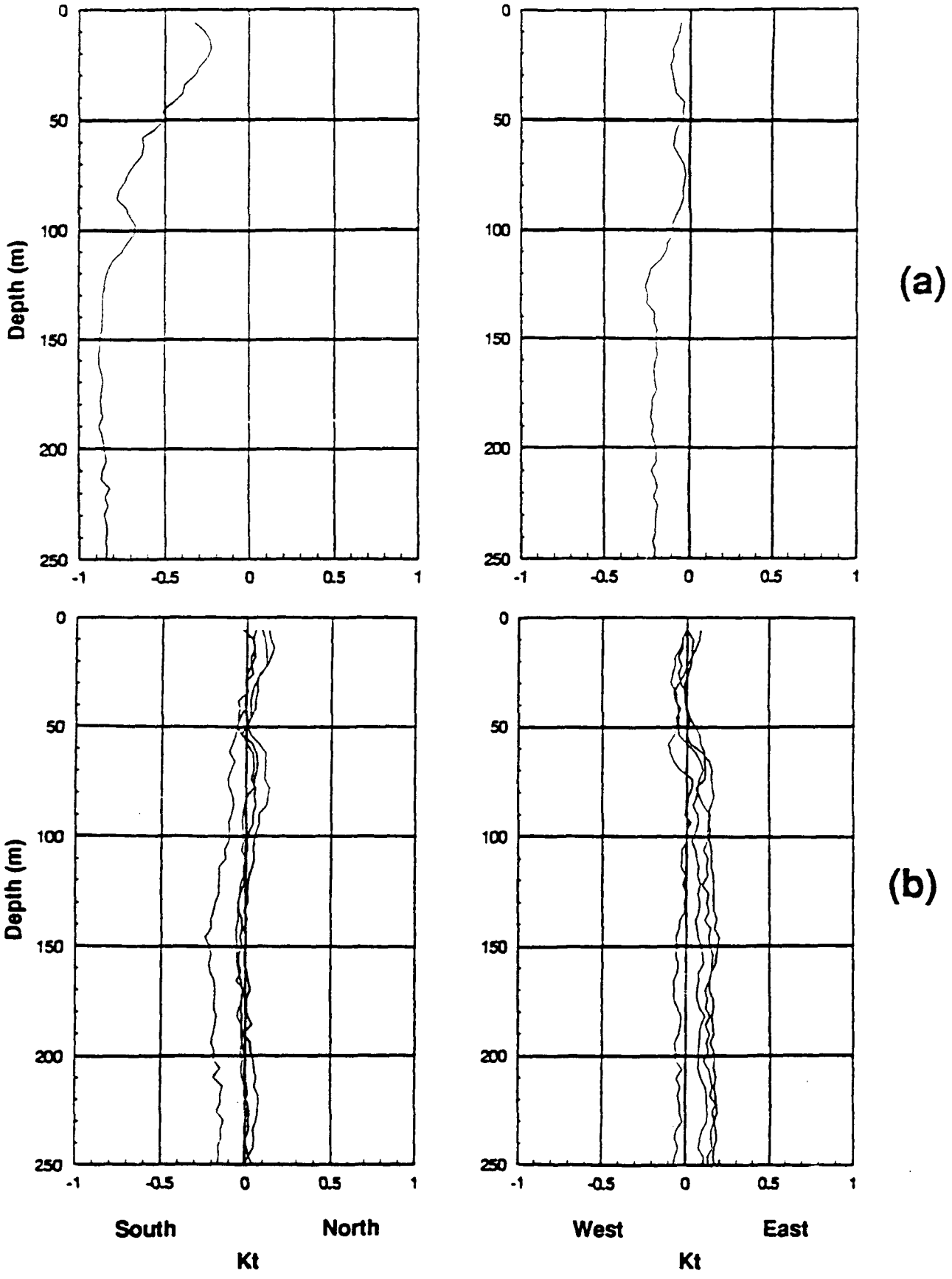


**Figure 33. Hourly averages of Acoustic Doppler Current Profiles between the hours of 0800 and 1800 when the vessel's speed was less than or equal to 0.5 kt, for (a) Station 17, and (b) Station 11.**

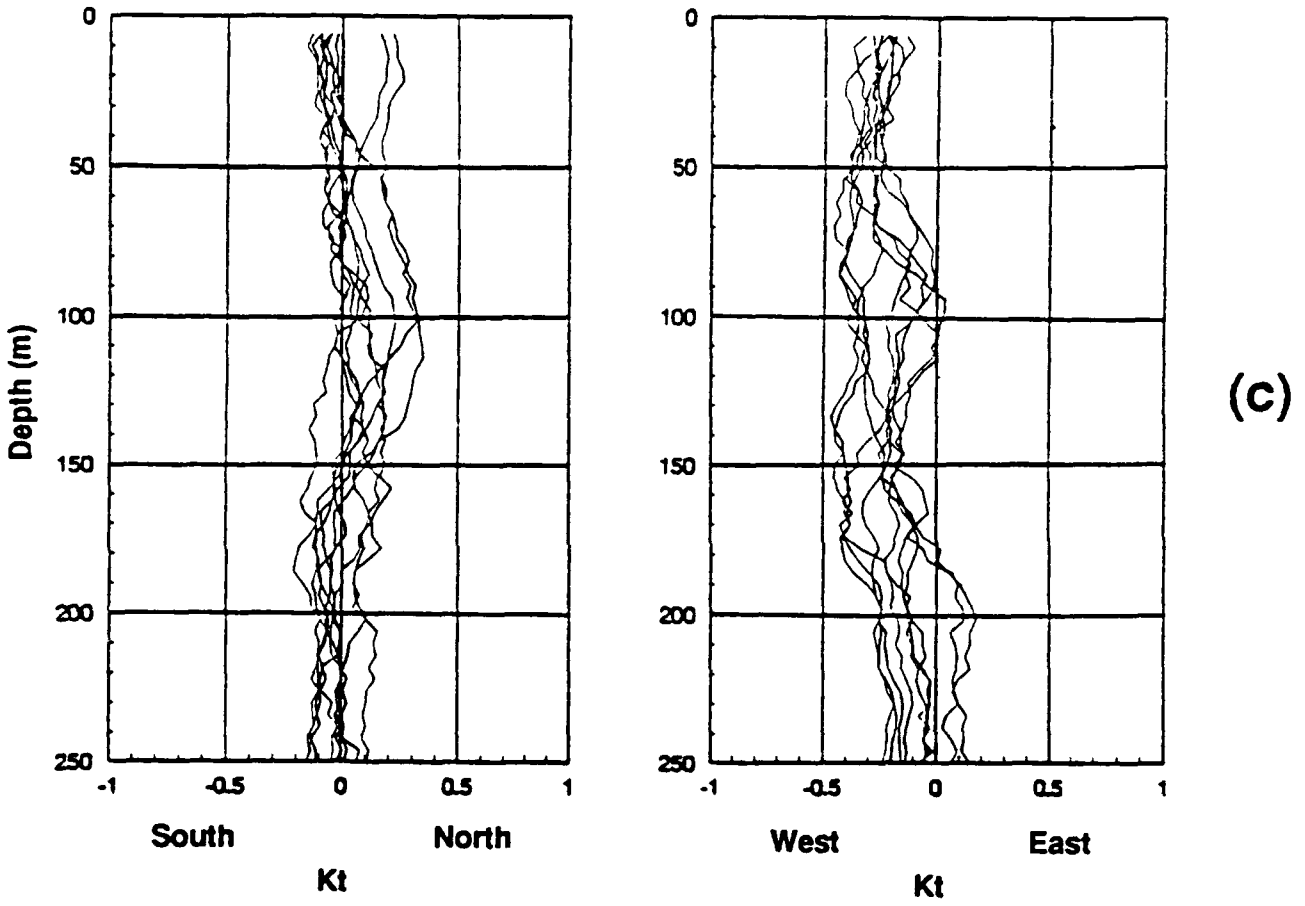


**Figure 33 *(continued)*. Hourly averages of Acoustic Doppler Current Profiles between the hours of 0800 and 1800 when the vessel's speed was less than or equal to 0.5 kt, for (c) Station 1.**

## 4.0 REFERENCES

Arnone, R., D.A. Wiesenberg, and K.D. Saunders (1990). The Origin and Characteristics of the Algerian Current. J. Geophpys. Res., 95(3), p. 1584-1598.

Bader, H. (1970). The Hyperbolic Distribution of Particle Size. J. Geophys. Res., 75(5), p. 2822.

Lavoie, D.M., D.K. Young, and M.S. Hulbert (1992). Bioluminescence in the Western Alboran Sea in April, 1991, Naval Oceanographic and Atmospheric Research Laboratory, SSC, MS, NOARL Technical Note 212.

Widder, E.A. (1991). Cruise Report P/V SEAWARD JOHNSON April 5-25, 1991 "Midwater Bioluminescence Assessment in the west Alboran Gyre (Mediterranean Sea)" Harbor Branch Oceanographic Institution Cruise Report (Ft. Pierce, FL).

**DISTRIBUTION LIST**

Asst. Secretary of the Navy
Research, Development, and
Acquisition
ATTN: CDR G. Berry
Pentagon Room 5E731, Code OCN
Navy Department
Washington, DC 20350-1000

Chief of Naval Operations
Department of the Navy
ATTN: OP-096T, Mr. R. Winokur
OP-021T2, R. Lauer
OP-021T2B, E. Hashimoto
Washington, DC 20350-2000

Office of Naval Research
ATTN: Code 112, Dr. E. Hartwig
Code 1123, Dr. R. Spinrad
Code 1123B, Ms. Mary Altalo
800 North Quincy Street
Arlington, VA 22217

Commanding Officer
Naval Research Laboratory Detachment
ATTN: Code 125L (10)
Code 125P (1)
SSC, MS 39529-5004

Commander
Naval Oceanography Command
ATTN: Code N2, CAPT Laduce
Code N532, J. Ownbey, Jr.
SSC, MS 39529-5000

Commanding Officer
Naval Oceanographic Office
ATTN: Code OP, V. Sprague
Code TD Library (2)
SSC, MS 39529-5001

Office of Naval Technology
ATTN: Code 23, CDR L. Bounds
800 North Quincy Street
Arlington, VA 22217

Commander
Space and Naval Warfare
Systems Command
ATTN: J. Griffin
2511 Jefferson Davis Highway
Building NC1
Arlington, VA 22202

Commander
Naval Undersea Warfare Center
Newport Division
ATTN: Code 8213, Dr. P. Temple
Newport, RI 02841

Commander
Submarine Group NINE
ATTN: LCDR B. Williams
Bremerton, WA 98315-5100

Commander, Sub Force
U.S. Atlantic Fleet
ATTN: Code 014, CDR T. Donaldson
Norfolk, VA 23511

Commander
Submarine Development Sqadron Twelve
ATTN: Code 225, LCDR E. Long
Box 70, Naval Submarine Base, New
London
Groton, CT 06340

Arete Associates
ATTN: Dr. T. Bell
P.O. Box 16287
Arlington, VA 22215

Applied Physics Laboratory
Johns Hopkins University
ATTN: Dr. C. Sinex
Johns Hopkins Road
Laurel, MD 20723-6099

University of California, Santa
Barbara
Marine Science Institute
ATTN: Dr. J. Case
Santa Barbara, CA 93106

Harbor Branch Oceanographic
Institute
ATTN: Dr. Edith Widder
Division of Marine Sciences
5600 Old Dixie Highway
Fort Pierce, FL 34946

# REPORT DOCUMENTATION PAGE

*Form Approved*
*OBM No. 0704-0188*



| 1. Agency Use Only *(Leave blank).* | 2. Report Date. | 3. Report Type and Dates Covered. |
|---|---|---|
| | March 1992 | Final |

**4. Title and Subtitle.**

Optical and Physical Characteristics of the western Alboran Sea: April 1991

**5. Funding Numbers.**

| | |
|---|---|
| *Program Element No.* | 0603704N |
| *Project No.* | R0118 |
| *Task No.* | 15003 |
| *Accession No.* | DN255001 |
| *Work Unit No.* | 13311D |

**6. Author(s).**

R. Hollman

**7. Performing Organization Name(s) and Address(es).**

Naval Oceanographic and Atmospheric Research Laboratory
Ocean Science Directorate
Stennis Space Center, MS 39529-5004

**8. Performing Organization Report Number.**

NOARL Technical Note 234

**9. Sponsoring/Monitoring Agency Name(s) and Address(es).**

Naval Oceanographic and Atmospheric Research Laboratory
ASW Oceanography Office
Stennis Space Center, Mississippi 39529-5004

**10. Sponsoring/Monitoring Agency Report Number.**

NOARL Technical Note 234

**11. Supplementary Notes.**

**12a. Distribution/Availability Statement.**

Approved for public release; distribution is unlimited.

**12b. Distribution Code.**

**13. Abstract** *(Maximum 200 words).*

The objective of this cruise was to characterize the bio-optical properties of the western Alboran Sea. This experiment involved the USNS BARTLETT, the R/V SEWARD JOHNSON and the JOHNSON SEA-LINK submersible (the latter two of the Harbor Research Oceanographic Institution). This technical note provides a first look report of the optical data acquired from 16 stations occupied by the USNS BARTLETT between April 2 and April 21, 1991. Results of the biological and bioluminescence experiments are covered in other reports.

**14. Subject Terms.**

Physical Oceanography, Optical Oceanography, Microstructure, Instrumentation

**15. Number of Pages.**

57

**16. Price Code.**

| 17. Security Classification of Report. | 18. Security Classification of This Page. | 19. Security Classification of Abstract. | 20. Limitation of Abstract. |
|---|---|---|---|
| Unclassified | Unclassified | Unclassified | SAR |